Spring 5-31-2001

Optical properties of photonic crystals

Anand G. Shenoy
New Jersey Institute of Technology

ABSTRACT

BAND -GAP CHARACTERISTICS OF 3D PHOTONIC CRYSTALS

by
Anand Shenoy

The ability to confine light in three dimensions has important implications for quantum optics and quantum-optical devices. Photonic crystals, the optical analog of electronic crystals, provide us a means of achieving this goal. This analogy has motivated a whole new series of experimental and theoretical searches for elusive photonic band-gap structures. Combinations of metallic and dielectric materials can be used to obtain the required three-dimensional (3D) periodic variation in the dielectric constant. This could pave the way for photonic crystal structures that have widespread applications.

The working of 3D photonic crystals into the wavelength regimes where most optoelectronic devices operate, i.e., 1.3 to 1.5μm was explored in the course of the thesis work. Simulations were run simultaneously on samples that were considered using Multirad. A one to one correspondence was sought between the two, i.e., experimental and simulated results. The basis for the conclusions was drawn from the known and present experimental results and simulations. The need for research on photonic crystal structures in particular areas was evaluated. Inferences drawn from this were then deployed to identify areas of modern science that would benefit from discoveries in photonic crystals.

OPTICAL PROPERTIES OF 3D PHOTONIC CRYSTALS

by
Anand Shenoy

A Dissertation
Submitted to the Faculty of
New Jersey Institute of Technology
in Partial Fulfillment of the Requirements for the Degree of
Master of Science in Electrical Engineering

Department of Electrical and Computer Engineering

May 2001

APPROVAL PAGE

OPTICAL PROPERTIES OF PHOTONIC CRYSTALS

Anand Shenoy

Dr. N M Ravindra, Thesis Advisor — Date
Professor of Physics, NJIT

Dr. Dentcho Ivanov, Committee Member — Date
Technical Director, Microelectronics Research Center, NJIT

Dr. William Carr, Committee Member — Date
Professor of Electrical Engineering and Physics, NJIT

Dr. Kenneth Sohn, Committee Member — Date
Professor of Electrical Engineering (1966) and Associate Chairperson of Electrical and Computer Engineering, NJIT

BIOGRAPHICAL SKETCH

Author: Anand Shenoy

Degree: Master of Science in Electrical Engineering

Date: December 2000

Undergraduate and Graduate Education:

- Master of Science in Electrical Engineering,
  New Jersey Institute of Technology, Newark, NJ, 2001

- Bachelor of Science in Electrical and Electronics Engineering,
  Manipal Institute of Technology, Mangalore, India, 1998

Major: Electrical Engineering

Publications

A. Shenoy, N. M. Ravindra, B. Sopori, O.H. Gokce, S. X. Cheng, L. Jin, S. Abedrabbo, W. Chen and Y. Zhang, "Emissivity Measurements and Modeling of Silicon Related Materials - AN OVERVIEW", International Journal of Thermophysics, 2001(In press)

This Thesis is dedicated to my family
Mrs. M Sundari Pai
Mr. K Gurudatt Shenoy
Mrs. Sheela Shenoy
Mr. Ajay Shenoy

ACKNOWLEDGMENT

The author wishes to express his sincere gratitude to his supervisor, Dr. N. M. Ravindra for the guidance, friendship and encouragement given throughout this research.

Special thanks to Dr. Dentcho. Ivanov, Dr. Kenneth Sohn and Dr. William Carr for serving as members of the committee.

The author is grateful to Sandia National Labs for having provided the samples, which were used, for analysis in the study.

The author is grateful to Prof. N. M. Ravindra for helping with grants (through a contract with NREL) to fund the research and for helping out throughout the research and also during the field trips.

The author appreciates the timely help and expert assistance from Mr. James Markham and Mr. Patrick Kenny in carrying out measurements on the samples.

And finally, a thank you to my colleagues, Aravind Balakrishnan and Vishal Mehta for their help and support throughout the course of the research.

TABLE OF CONTENTS

TABLE OF CONTENTS
(Continued)

Chapter **Page**

TABLE OF CONTENTS
(Continued)

Chapter **Page**

LIST OF TABLES

Table **Page**

LIST OF FIGURES

LIST OF FIGURES
(Continued)

Figure **Page**

LIST OF FIGURES
(Continued)

Figure **Page**

CHAPTER 1

INTRODUCTION

Have you ever wondered what happens to electrons in semiconductor crystals or more so in particular photonic crystals? If not then consider these facts. There are forbidden energy states in a bandgap of the photonic crystal and because of the interference of electron wave functions in the crystal lattice certain effects can be observed[1]. Scattering at periodically arranged "dielectric atoms" might lead to an optical bandstructure, which fundamentally alters the propagation of light as well as emission and absorption processes in these mostly artificial structures. So it would good to consider a close analogy of photons in so-called photonic crystals with other such related phenomena in the InGAS range of spectrum i.e. 1.3 to 1.8microns.

Initial efforts[2] were motivated by the prospect of a photonic band gap, a frequency band in three-dimensional dielectric structures in which electromagnetic waves are forbidden irrespective of the propagation direction in space. An article in the Science magazine[3] said, "photonic crystals, tiny lattice-like structures that channel photons, may pave the way for computers that calculate at light speed". The British Broadcasting Corporation (BBC) [4] hinted that "this year, scientists made significant steps in their quest to harness the power of photons in the same way that electrons are used in electronic circuits". This year researchers have built photonic crystals and components, which can manipulate light waves just as semiconductors manipulate electrical current and this would lead to new types of high speed computers (next generation) and high speed communication circuits capable of handling huge volumes of data, audio and video signals.

The friction between the photonic-band-gap and thin-film schools has appeared before. Main advantages of these structures are high conductivity, high transparency, a wide pass band, and the ability to tune the transmission window over a wide range of wavelengths. Fabrication techniques are well established and relatively cheap, and there are many potential applications, applications that could replace ITO coatings[4] in display technology, polymer lasers and polymer electro-optic modulators. Other applications include UV blocking, IR reflective windows, optical interconnects, and wide and band pass filters. The nonlinear optical properties of such materials should also prove promising. Though all this is promising, work in this field is still in the infant stages. Photonic crystals may pave the way for making cheaper, smaller, more efficient wave containers and guides than other materials known for optical communications, and may advance the day of optical computing.

Since first being introduced more than 10 years ago[5], the concept of photonic bandgap has attracted increased attention in the scientific community. Over 500 research groups are involved currently in the studies of photonic band gap crystals. Light has several advantages over electrons in the quest for ever-smaller integrated circuits[6]. But, all optical and optoelectronic circuits have had little impact, largely because of a lack of a multipurpose optical component analogous to the electronic transistor. Light can travel in a dielectric material at much greater speeds than an electron in a metallic wire. Light also holds the capabilities to carry a large amount of information per second. The bandwidth of dielectric materials is significantly larger than that of metals: the bandwidth of fibre-optic communication systems is typically of the order of 100 gigahertz, while that of electronic systems (such as the telephone) is only a few hundred kilohertz. Furthermore,

light particles (or photons) are not as strongly interacting as electrons, which helps reduce energy losses.

Photonic crystals, consisting of various materials of varying dielectric properties, which are designed to affect the behavior of photons in the way that semiconductors manipulate electrons, could one day fulfil the same role as that of electrons. Photonic crystals are materials patterned with a periodicity in dielectric constant, which can create a range of 'forbidden' frequencies called a photonic bandgap[7]. Photons with energies lying in the bandgap cannot propagate through the medium. This provides the opportunity to shape and mould the flow of light for photonic information technology.

For the past 50 years, semiconductor technology has played a significant role in almost every aspect of our daily lives. The drive towards miniaturization and high-speed performance of integrated electronic circuits has stimulated considerable research effort around the world. Unfortunately, miniaturization results in circuits with increased resistance and higher levels of power dissipation, and higher speeds lead to a greater sensitivity to signal synchronization. In an effort to further the progress of high-density integration and system performance, scientists are now turning to light instead of electrons as the information carrier[8].

In spite of the numerous advantages of photons, all-optical circuits have yet to be commercially available on a large scale. Some hybrid optoelectronic circuits have produced significant improvement over the performance of electronic circuits, but the difficulties in designing a multipurpose optical component analogous to the electronic transistor has severely hindered the proliferation of all-optical systems. A new class of optical material structures known as photonic crystals[9] may hold the key to the continued

progress towards all-optical integrated circuits. Scientists have begun to propose and integrate photonic discoveries with integrated circuits, which resemble microscopic metropolises at micrometer length scales, with photonic crystal buildings that house bundles of light, and highways and bridges that guide light along narrow channels and around tight corners. The analogy between electromagnetic wave propagation in multidimensional periodic structures and electron wave propagation in real crystals has proven to be a fruitful one[10].

1.1 Types of Photonic Crystals

Photonic Crystals have been put through a number of processes in recent years and are used in a wide range of industries from optics to communications. Photonic crystals can be mainly classified under three groups: One Dimensional Photonic Crystals (1D Photonics), Two Dimensional Photonic Crystals (2D- Photonics) and Three Dimensional Photonic Crystals (3D Photonics) [11].

1.1.1 One Dimensional Photonic Crystals

The Fig. 1.1 shown in the next page is a one-dimensional photonic crystal, which is similar to a Bragg Stack. If a wave packet is incident normal to this structure, i.e. perpendicular to the first flat face, the transmittance is as shown in Fig. 1.2. The normalized frequency used in all the spectra that follow, is the ratio of that particular frequency to the center frequency.

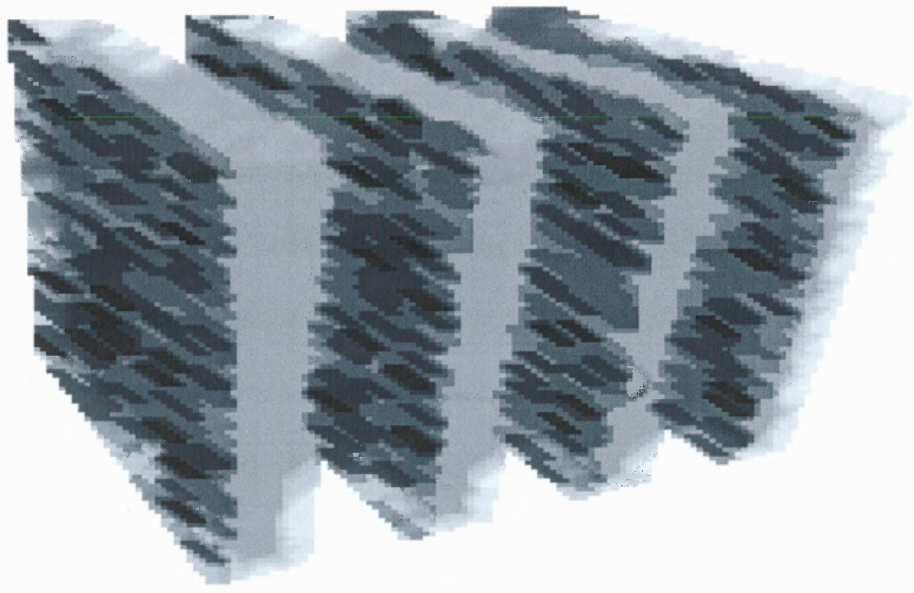

Figure 1.1 Structure of a One Dimensional Photonic Crystal1[12]

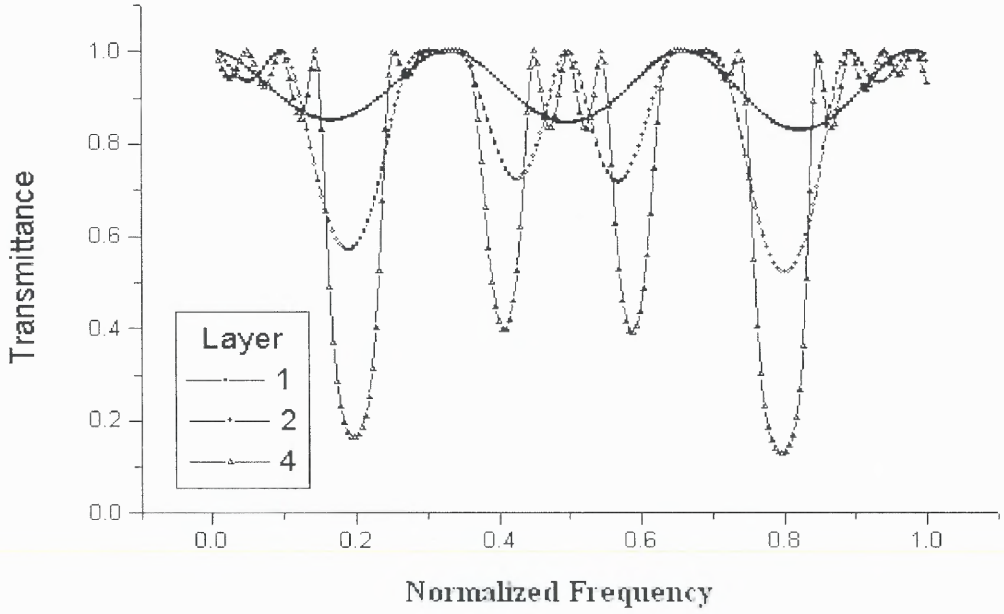

Figure 1.2 Transmittance Vs Normalized Frequency for a few layers of the crystal[12]

As can be seen in Figure 1.2, with increase in crystal thickness, the transmission response for some frequencies rapidly approaches zero. However, at the same time, the widths of these troughs decrease. One-dimensional systems in photonic crystals are actually tailor made to provide either reflection or anti-reflection coatings. This is done by careful choice of the materials used, their thickness and the number of layers.

One of the other tools frequently used with the photonic band gap (PBG) subject area is that of the band structure diagram. In order to introduce this concept, the best example would be one dimension. One of the most important relations in electromagnetics, especially in reflection to PBG (Photonic Band Gap) apart from Maxwell's Equations is the dispersion relation:

$$\omega n = c k$$

(ω=angular frequency, n=refractive index, c=speed of light in vacuum, k=wave vector). To start with, consider a 'piece' or 'block' of air. We do not have to worry about waveguides or bits of metal or PBG crystal for the moment. For the sake of comparison and for comprehension, what happens can be seen if a block of dielectric material and not air is present. What modes are present then?

From the two diagrams in Fig. 1.3, it can see that there is a diamond shape that repeats. The number of diamonds is different between the air and dielectric, because in free space dispersion relation wn=ck, if n is changed, then the gradient of the line changes. Since a block of air has been chosen with an artificial periodicity, the expected straight line of gradient gets folded up. When it reaches the side of the plot, it continues with the same gradient by folding and this explains the diamond shape.

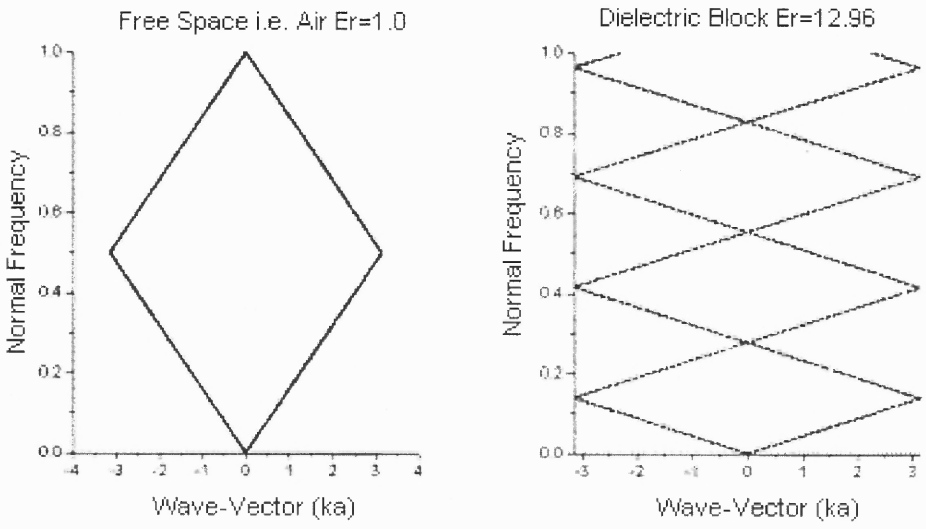

Figure 1.3 Air and Dielectric Block Band Diagrams[12]

The Bragg stack[12] mentioned above is a mixture of two materials, and if the ratios are right, then useful gaps in the band diagram, which are the called "Photonic Band Gaps" are created. It can be concluded from the band diagrams and transmission plots that, if materials, along with their associated dielectric constants and their thickness are chosen correctly, useful PGBs can be obtained. One dimensional photonic band gap structures such as 'Bragg Stacks' are used within laser cavities and for optical coatings. Generally, a one dimensional gap is only of use if the application is going to be restrained to a specific, or small range of angles for a source embedded within the dielectric medium.

1.1.2 Two Dimensional Photonic Crystals

There is a substantial interest in these structures at present. There are many types of two dimensional lattice structures, namely - square lattice, hexagonal lattice, honeycomb lattice, etc.

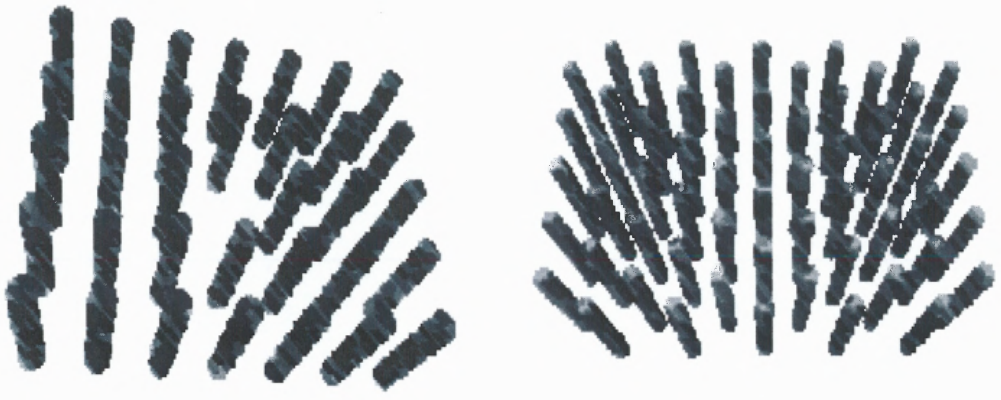

Figure 1.4 Examples of 2D Lattice types with cylinders[12]

A two-dimensional gap means that if a wave is incident on the structure from any direction within the same two-dimensional plane as the periodicity of the crystal, then it will always be reflected. This, of course, is limited to a range of frequencies. But quite reasonable band- width (band width = gap width / central gap frequency) can still be achieved. Repetitive rows of periodically spaced cylinders ensure that the two dimensional periodicity holds in only one plane. Therefore, if the incident radiation is restricted to this plane, then for the correct filling ratios and material constants and polarization of the wave, a complete two-dimensional band gap can be observed. Within the two-dimensional plane, it does not matter from which angle the structure is bombarded. Outside the plane, the special periodicity that has been deliberately set up

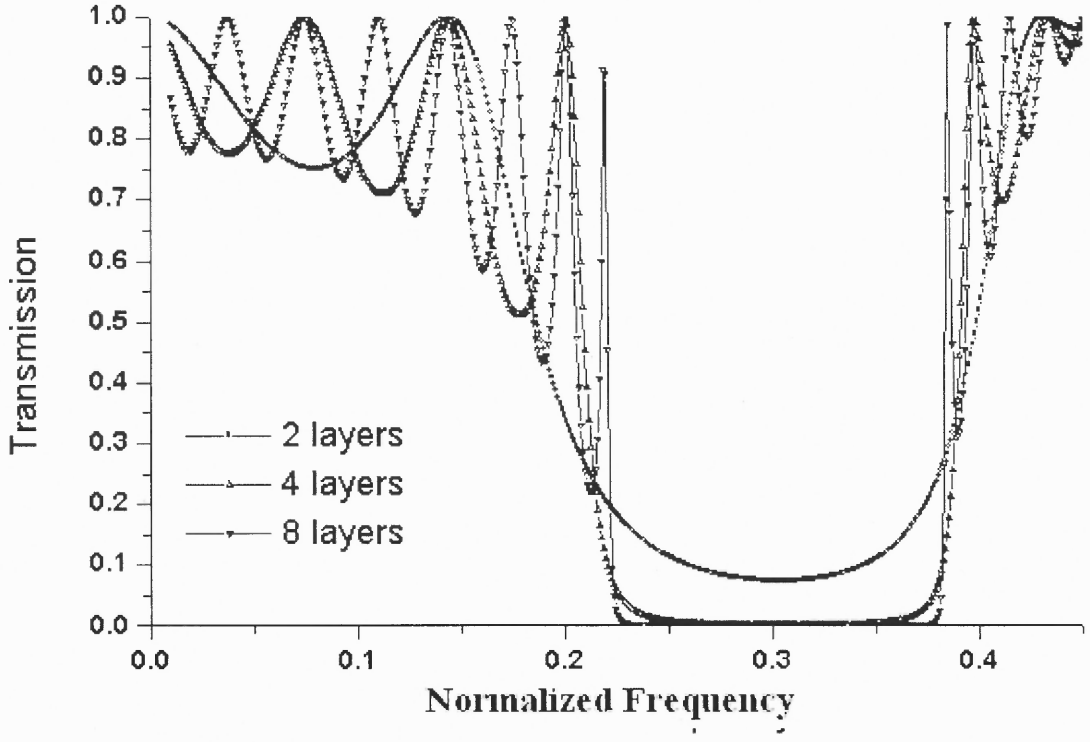

Figure 1.5 Transmission Vs Normalized Frequency for a two-dimensional Lattice Perfect Structure[12]

becomes increasingly compromised. Consequently, a marked decrease is seen in the photonic band gap behavior. The graph shown in Fig. 1.5 is for a perfect lattice. There are no spikes in the region where there is normally zero transmission (as in the case of lattices with defects).

1.1.3 Three Dimensional Photonic Crystals

Three-dimensional photonic crystals provide three-dimensional gaps. This is to say, any wave from any direction will be completely reflected. The combination of three-dimensional photonic crystals and integrated planar antenna technology provides a new exciting approach to a range of advanced efficiency enhanced antenna systems for the

future. They may provide a novel reflector technology that can be easily scaled in size to fit almost all intended applications. Take, for example, the third structure shown below. A periodic pattern is etched onto each wafer. The wafers are then stacked vertically, with each consecutive layer being rotated with respect to the previous one. This results in a woodpile like structure.

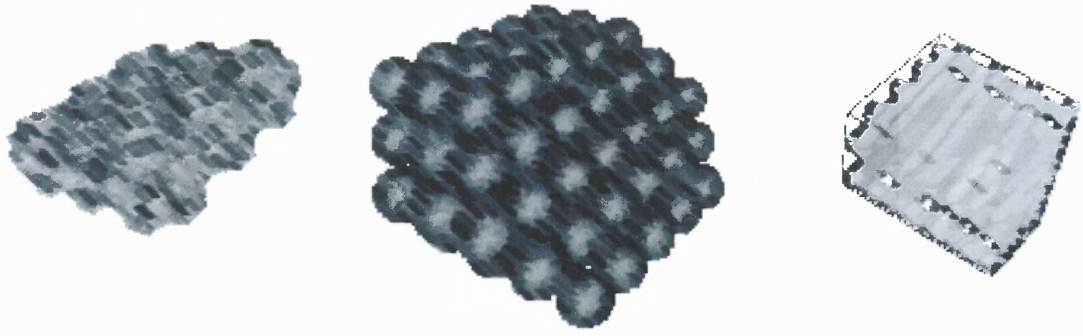

Figure 1.6 Structure of the lattice for Inverted Opal <001>, Close Packed Opal <111>, Woodpile System[12]

1.2 Thesis Content

The main objective of this thesis is to explore the numerous possibilities that could arise out of the phenomena of light trapping between the layers in a photonic crystal. By working on the 3D photonic crystal, it can be brought into the wavelength regime, where most optoelectronic devices operate, i.e. 1.3 to 1.5 μm. A variety of exciting photonic devices, including low-loss waveguide sharp bends, high-Q resonant cavities and single-mode LEDs can now be made from 3D photonic crystals. Using photonic band gap materials, one can fabricate dielectric waveguides and high Q-resonators for solid state laser devices. Also, light trapping could have important implications for quantum optics and quantum-optical devices like the modification of blackbody radiation, the

localization of light to a fraction of a cubic length etc. The main objective is the search for a structure that will display the much needed characteristics in the infrared wavelength range, so that such a material can be used to construct lasers in that particular range. In doing so, the work presented in this thesis will focus on the analysis of certain samples of photonic crystals. Transmissivity measurements, in particular, will be analyzed towards the end of this thesis. To realize most of the applications, it is crucial to have a photonic-band-gap crystal lattice that can be easily and reproducibly fabricated.

CHAPTER 2

BACKGROUND AND SIGNIFICANCE OF STUDIES ON PHOTONIC CRYSTALS

Photonic crystals are periodic structures that, through interference, prevent certain electromagnetic waves from propagating through the structure. The crystals are of interest to designers of optoelectronic devices since they efficiently confine energy in a desired wavelength region. Because crystal structures must be built at the same scale as the wavelength to be suppressed, the difficulty of producing photonic crystals increases with higher frequencies. As a result, most successful demonstrations of the principle have used millimeter and microwaves. Photonic Crystals present a tremendous opportunity for the future; they reduce the mass of a system, increase the efficiency and are simple to manufacture all features that are essentially antenna systems. Photonic crystals are structures that restrict the propagation of particular wavelengths of light through destructive interference. These forbidden wavelengths, as in electronics, are defined as being within the bandgap of the structure and the crystals are often also known as photonic bandgap materials.

According to an article in the Nature, a few developments could mark an important advancement in the field and could lead to applications such as ultrafast optical switching, guiding light on a semiconductor chip and constructing efficient microlasers. These photonic crystals, which measure less than half a micron, are different from other photonic crystals in several respects. Bragg gratings, for example, are one-dimensional and have a larger cavity. The size of the microcavity inside the three-dimensional crystals is much smaller, making them suitable for highly efficient nanolasers. By introducing

doping elements, physicists increase the density of electromagnetic states within the crystal at one specific frequency. At that frequency, the atoms inside the crystal will undergo a faster spontaneous emission (or faster rate of recombination). When atoms undergo this transition, photons will bounce back and forth against the crystal walls, which function like mirrors. A fraction of the light then escapes from the crystal.

2.1 Properties of Photonic Band Gap Materials

Since the invention of the laser, the field of photonics has progressed through the development of engineered materials, which mold the flow of light[13]. Photonic band gap (PBG) materials are a new class of dielectrics, which are the photonic analogues of semiconductors. The photonic band gap is equivalent to a frequency interval over which the linear electromagnetic propagation effects have been turned off. Unlike semiconductors, which facilitate the coherent propagation of electrons, PBG materials facilitate the coherent localization of photons[14]. Applications include zero-threshold micro-lasers with high modulation speed and low threshold optical switches and all-optical transistors for optical telecommunications and high-speed optical computers. In a PBG, lasing can occur with zero pumping threshold. Lasing can also occur without mirrors and without a cavity mode since each atom creates its own localized photon mode. This suggests that large arrays of nearly lossless microlasers for all optical circuits can be fabricated with PBG materials. Near a photonic band edge, the photon density of states exhibits singularities, which cause collective light emission to take place at a much faster rate than in ordinary vacuum. Microlasers operating near a photonic band edge will exhibit ultrafast modulation and switching speeds for application in high-speed data

transfer and computing. Applications such as telecommunications, data transfer, and computing will be greatly enhanced through all-optical processing in which bits of information, encoded in the form of a photon number distribution, can be transmitted and processed without conversion to and from electrical signals. The PBG material provides dopant atoms with a high degree of protection from damping effects of spontaneous emission and dipole dephasing. In this case, the two-level atom may act as a two-level quantum mechanical register or single photon logic gate for all optical quantum computing.

A collaboration between researchers in Germany, the US, and Greece has led to the development of a new way to fabricate photonic crystals[15]. The technique, based on the LIGA process, has produced lattices made up of cylinders that are just a few tens of microns across. These structures are made of ceramics; more recently, attempts have been made to use both ceramics and metals. Researchers have concluded that the latter materials should be useful for high-quality bandpass filters.

Photonic crystals that operate in the visible spectrum have been generated via a technique that is intrinsically fast and, if some materials issues can be resolved, it can be relatively inexpensive. Researchers at the University of Oxford[12] have used holography to create three-dimensional molds that, once inverted by being filled with high-index materials and the original structure scrapped, have a photonic bandgap useful for some optoelectronic devices. Though the method has not yet been perfected, researchers are hopeful that holographic fabrication, with its inherent flexibility, will make the use of photonic crystals more practical. This work was carried out in Oxford's physics and chemistry departments and led by Andrew Turberfield and Bob Denning[12].

Scientists at Sandia have devised the first 3D photonic crystal operating at a wavelength of 1.5-micron (the all- important preferred wavelength for light traveling in optical fibers). Repeatedly layering and etching films of different dielectric constants has led to the fabrication of the vertical topology of the structure. For one layer of the photonic crystal, first SiO_2 is deposited, masked and then etched to achieve the desired depth. The resulting "trenches" are filled with polycrystalline silicon. In the last process step, the surface is polished. Then the entire process is repeated in order to obtain multilayers. In the final step, the wafer is submerged in an HF/water solution to remove the SiO_2.

The specifications of the structure are as follows:

distance between two parallel bars = 4.2 micrometers;

width of a bar = 1.2 micrometers;

thickness of layers = 1.6 micrometer.

The smoothness of the PGB crystal is controlled within 1% of the layer thickness above the wafer. The crystal is cut down to 1 x 1 cm, which corresponds to 2400 rods per layer. The band gap with a 12.5-micrometer wavelength extends over 1 micrometer. With further optimization of the fabrication process, it should be possible to create a crystal with a difference of 2 in the refractive indices. In this case, layers of Si_3N_4 can be used in the photonic crystal. Photonic crystals will be components in future optical transistors--- by deflecting light, they will be able to act as optical switches; by trapping light, they will be able to produce optical amplification within cavities. The crystals will also be part of other optical integrated circuit components such as low-power nanolasers and waveguides.

Chigrin and Lavrinenko in collaboration with the Institute of Molecular and Atomic Physics, Belarus National Academy of Sciences, have found out that under certain conditions, a one-dimensional photonic crystal can exhibit total reflection for all incident angles and any polarization[16]. A one-dimensional photonic crystal is a well-known dielectric mirror consisting of alternating layers with low and high indices of refraction. In contrast to the 3D microstructures, 1D dielectric lattices are unique. Using modern technology, it is possible to produce

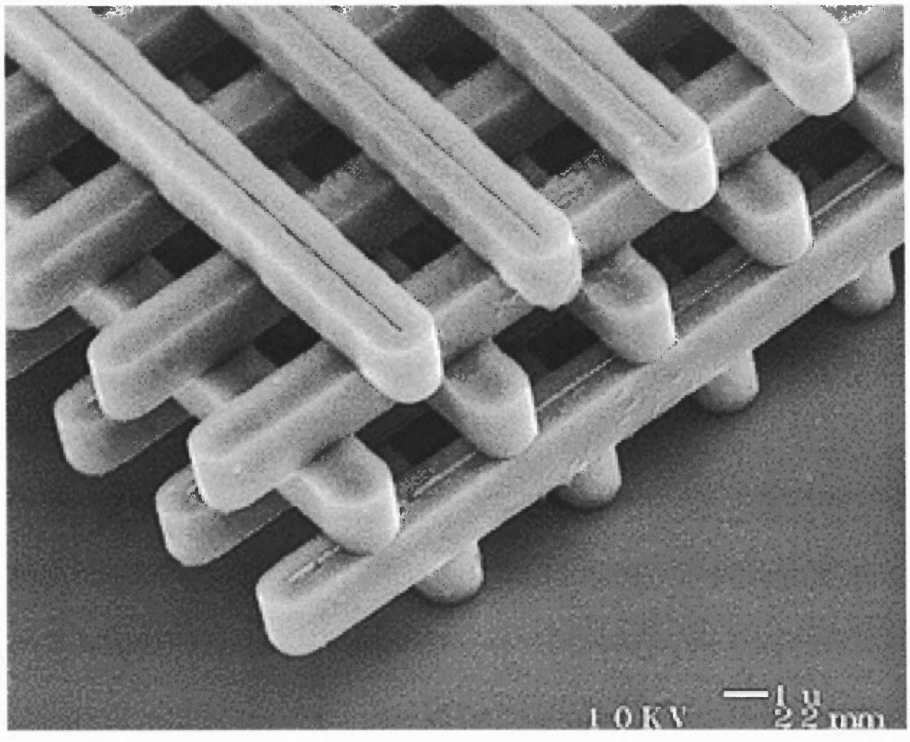

Figure 2.1 Structure of the 3D photonic crystal fabricated at Sandia[5]

the desired wavelength-scale for various applications. An inexpensive alternative possibility to control the propagation of light in applications such as optical communications becomes viable. At optical frequencies, all-dielectric thin-film

omnidirectional totally reflecting mirrors can be used as enclosure coatings for high finesse microcavities, where lossy metallic mirrors cannot be used. Many other applications that can benefit from these capabilities open up. Among these are frequency filters, microwave antenna substrates, enclosure coatings of waveguides, etc.

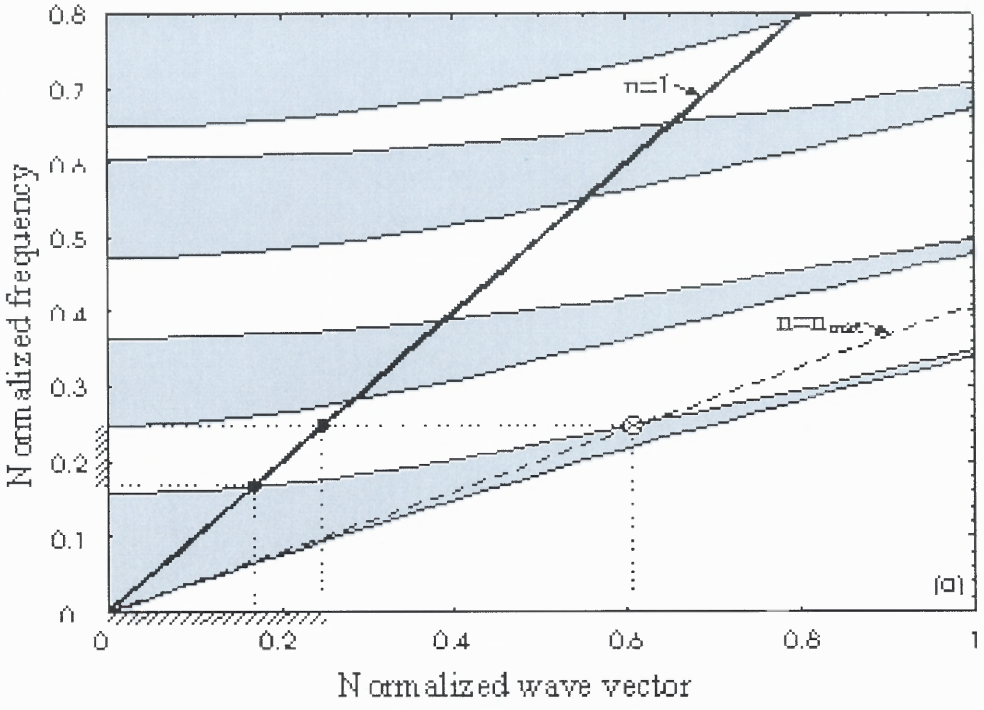

Figure 2.2 The photonic band structure for a typical 1D photonic crystal[5]

The photonic band structure for a typical 1D photonic crystal is shown in Fig. 2.2 for TE and TM waves, respectively. The main feature of all 1D photonic crystals is that although forbidden gaps exist for most given values of the tangential component of the wave vector, there is not an absolute nor complete photonic band gap if all possible values of the tangential component of the wave vector are considered[17]. However, when a plane electromagnetic wave illuminates a 1D semi-infinite photonic crystal, the tangential

component of the wave vector remains constant throughout the crystal. The tangential component of the wave vector lies between zero for normal incidence and (n w / c) for grazing incidence. Therefore, only values of the tangential component of the wave vector, which are inside the range, need to be considered. For this limited range (the shaded area on the wave vector axis), there is the frequency region (the shaded area on the frequency axis) which is completely inside the forbidden gaps of the photonic crystal both for TE and TM polarization. No propagating mode is allowed in the photonic crystal for any propagating mode in the ambient medium within this frequency region. The total omnidirectional reflection arises for both TE and TM polarization[18].

Though conceptually simple, photonic crystals have been difficult to fabricate for operation in the visible spectrum because the feature sizes involved have to be of the order of the wavelengths of visible light if they are to work. Though IC microlithography can now reach the required resolution, the crystals produced are limited in depth, which restricts their effectiveness. The new technique does not have those restrictions. Instead of building up a series of patterns on a substrate, the entire three-dimensional crystal is recorded at once by causing an interference of four coherent laser beams. By choosing the appropriate direction, intensity and polarization relationships among them, the structure of the resulting interference pattern can be manipulated as required. The key to this new generation of optoelectronic devices lies in the design of the photonic crystal materials, which may be used to control the light - or indeed any electromagnetic radiation. These are composites, made of two materials with different refractive indices, organized into a periodic structure in three dimensions. If the periodicity is comparable in its length scale with the wavelength of light, say around 0.5 micrometers, then there are

'band gaps', i.e. frequency bands in which propagation is not allowed, and the photonic crystal is a perfect reflector. The real technological interest lies in the properties of defects in the crystal, which create localized electromagnetic modes at certain defined frequencies in the band gap. These defect modes can be controlled to form a very efficient laser, a photonic switch or a waveguide. Such waveguides could incorporate very sharp bends on the micron scale thereby allowing the construction of microscopic photonic integrated circuits.

2.2 Simulation methods of Photonic Crystals

A joint effort between the Condensed Matter Physics group, the Microelectronics Research Center, and the Department of Materials Science and Engineering at Oxford has been investigating photonic crystals and their properties. These materials may have photonic band gaps (PBG) in the microwave, millimeter, infrared, or optical wavelengths depending on their physical dimensions. The fabrication of photonic crystals with gaps in the optical wavelengths is being pursued. Either colloidal systems or advanced silicon processing techniques are used (silicon processing has been performed by Lin's group at Sandia Labs). Secondly, in the microwave and millimeter wavelengths (where photonic crystals already exist), antennas made from photonic crystals[25], waveguides in photonic crystals, and filters using photonic crystals are being fabricated. The theoretical investigations have led to experimental fabrication and testing of new structures, which in turn drive further advances in their design.

2.2.1 Transfer Matrix Method

Theoretical studies using the Transfer Matrix Method (TMM)[29] have been crucial to the design and characterization of these PBG materials. TMM calculates the transmission and reflection coefficients of a plane wave incident on a PBG structure. It is computationally very demanding, with simulations covering long time spans and requiring large system sizes, especially for studying defects and disordered states. The TMM code is run on a Cray T3E, as well as an older Paragon and some clusters of workstations. The larger memory and faster processors in the Cray T3E and IBM SP permit to simulate much larger systems and further the ability to study disordered systems.

2.2.2 Finite Difference Time Domain method

Utilizing a Fabry Perot cavity between two photonic crystals, an exceptionally directional antenna can be fabricated. Using a dipole antenna source within the cavity, exceptionally directional beams can be obtained from the antenna, at the resonant frequency of the cavity. The beam has a half power width of less than 10° when compared to the normal. Finite-difference simulations are used to design a planar waveguide in the 3-dimensional layer-by-layer crystal with a 90° bend with 100% transmission through the bend. A similar L-shaped waveguide has also been simulated using a metallic photonic crystal with only 3 unit cells thickness needed for 85% transmission efficiency. The performance of waveguides in two-dimensional PBG structures has been simulated and the guiding efficiency is optimized as a function of the structural parameters. Such structures are important in all-optical photonic crystal devices.

2.3 Performance of the FDTD code

The FDTD code[29] uses a typical finite difference method with a 2D spatial decomposition. This requires passing data to the 4 neighboring nodes during each iteration. The communication load is fairly small compared to the computational load, so this code scales very well on even the most challenging multiprocessor machines. The scaling curves shown here are for a small cluster of 64 PCs connected only with Fast Ethernet. This demonstrates that the code scales well even for small system sizes on a cluster where the interprocessor communication rate is much lower than for traditional MPPs such as the Cray T3E and IBM SP. On these larger systems, this code scales ideally to very large numbers of nodes.

2.4 Waveguide Bends in Photonic Crystals

In conventional waveguides such as fiber-optic cables, light is confined by total internal reflection (also known as index confinement, a more accurate term when the guide diameter is on the order of the wavelength) [20]. One of the weaknesses of such waveguides, however, is that creating bends is difficult. Unless the radius of the bend is large compared to the wavelength, much of the light will be lost. This is a serious problem in creating integrated optical "circuits," since the space required for large-radius bends is unavailable.

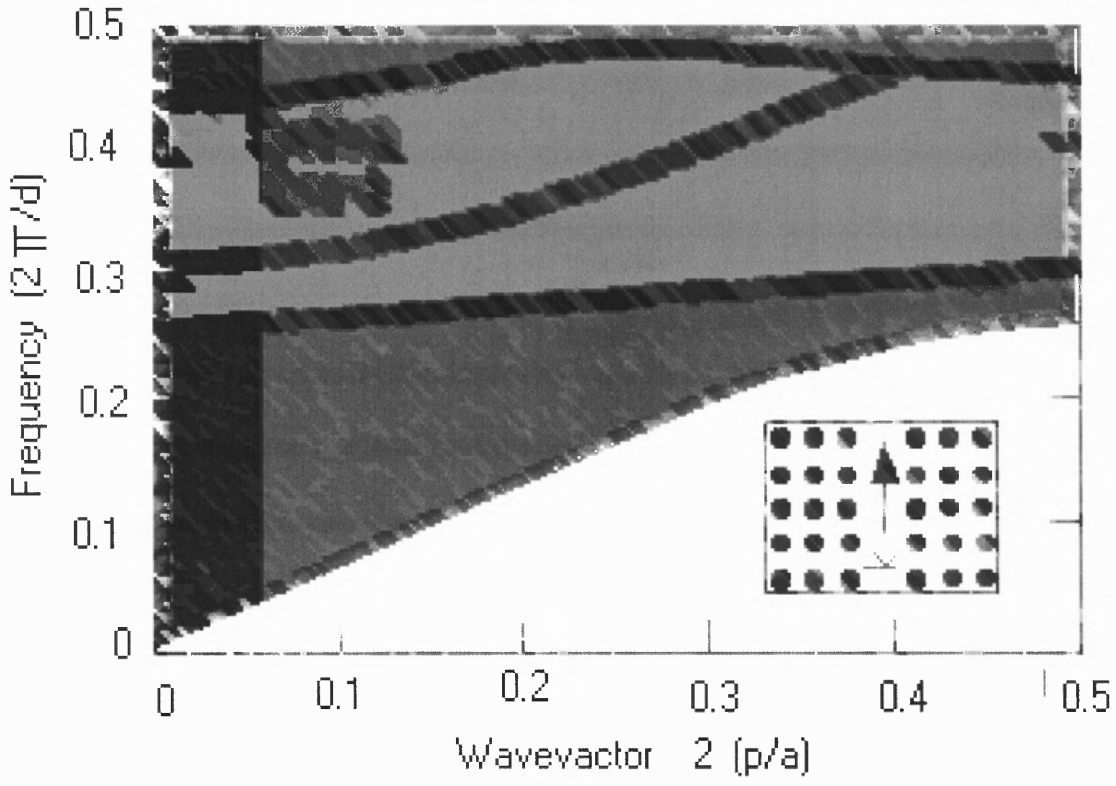

Figure 2-3 Structure of a 2D photonic crystal[25]

Photonic crystal waveguides operate on a different principle. A linear defect is created in the crystal, which supports a mode that is in the band gap. This mode is forbidden from propagating in the bulk crystal because of the band gap. (That is, waveguides operate in a manner similar to resonant cavities, except that they are line defects rather than point defects). When a bend is created in the waveguide, it is impossible for light to escape (since it cannot propagate in the bulk crystal). The

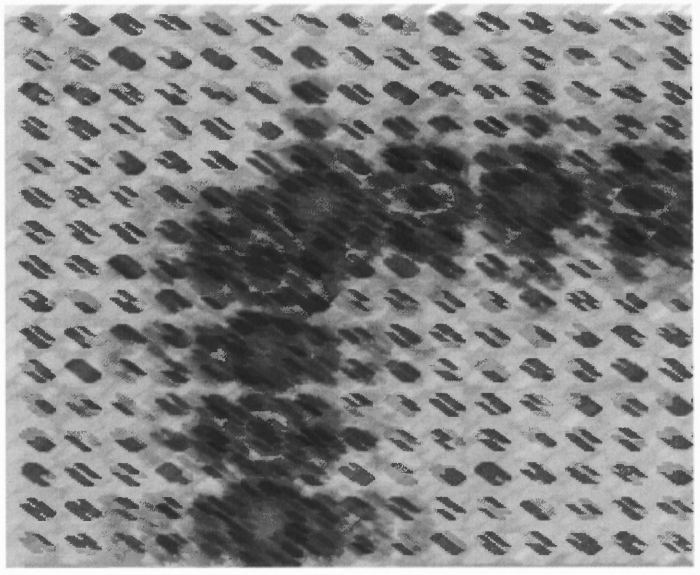

Figure 2-4 Electric filed in a waveguide exhibiting 100% transmission[25]

only possible problem is that of reflection. However, the problem can be analyzed in a manner similar to one-dimensional resonant tunneling in quantum mechanics, and it turns out to be possible to get 100% transmission. The above fig. 2.4 depicts the electric field in a waveguide bend exhibiting 100% transmission.

2.5 Resonant Cavities in Photonic Crystals

When a point defect is created in a photonic crystal, it is possible for that defect to pull a light mode into the band gap[26]. Because such a state is forbidden from propagating in the bulk crystal, it is trapped. The mode decays exponentially into the bulk. Such a point defect, or resonant cavity, can be utilized to produce many important effects. For example, it can be coupled with a pair of waveguides to produce a very sharp filter (through resonant tunneling). Point defects are at the heart of many other photonic crystal devices, such as channel drop filters. Another application of resonant cavities is

enhancing the efficiency of lasers, taking advantage of the fact that the density of states at the resonant frequency is very high (approaches a delta function). By changing the size or the shape of the defect, its frequency can easily be tuned to any value within the band gap. Moreover, the symmetry of the defect can also be tuned. By increasing the amount of dielectric in the defect, one can pull down higher-order modes, corresponding to the s, p, d, etc states in atoms.

An image of a fabricated air bridge structure is presented in fig. 2.5. This is a conventional waveguide, surrounded by air, into which a regular set of holes have been punched (the center to center spacing between the holes is 1.8μm). The periodic structure provided by these creates a band gap, i.e. a one-dimensionally periodic photonic crystal (often referred to as simply a "one-dimensional" photonic crystal, although it exists in three dimensions). In the center of the bridge, a slight defect in the crystal has formed leaving out an extra space between the holes. This forms a resonant cavity, which can be used as a filter.

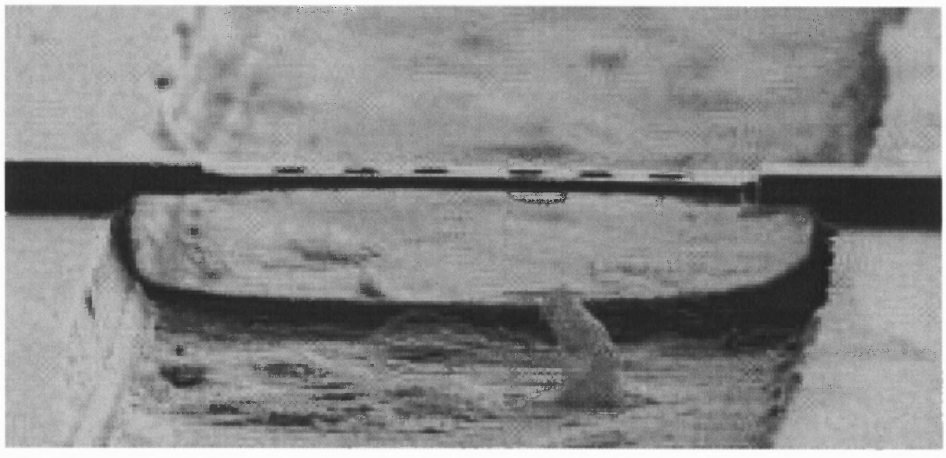

Figure 2-5 Resonant cavity in a Photonic Crystal[25]

2.6 Perfect Channel Drop Filters

An important device for optical communications and in many other applications is a channel-drop filter. Given a collection of signals propagating down a waveguide (called the bus waveguide), a channel-drop filter picks out one small wavelength range (channel) and reroutes (drops) it into another waveguide (called the drop waveguide). For an example of how this is useful, imagine an optical telephone line carrying a number of conversations simultaneously in different wavelength bands (i.e. using wavelength division multiplexing). Each conversation needs to be picked out of the line and routed to its destination, and to separate a conversation you need a channel-drop filter. It turns out that by using photonic crystals, one can construct a perfect channel drop filter--that is, one which reroutes the desired channel into the drop waveguide with 100% transfer efficiency (i.e. no losses, reflection, or crosstalk), while leaving all other channels in the bus waveguide propagating unperturbed.

2.7 Perfect Waveguide Intersections

In constructing integrated optical "circuits," space constraints and the desire for complex systems involving multiple waveguides necessitate waveguide crossings. We propose a novel method for intersecting waveguides with negligible crosstalk. Moreover, this technique depends on general symmetry considerations that can be applied to almost any system a priori, with little need for manual "tuning." The basic idea is to consider coupling of four branches, or "ports" of the intersection in

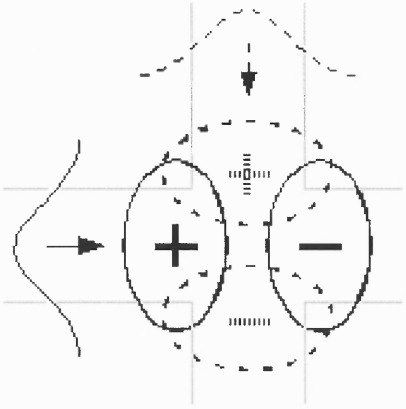

Figure 2-6 A perfect waveguide intersection

terms of coupling through a resonant cavity at the center. If the resonant cavity can be prevented by symmetry from decaying into the crossing waveguide, then the situation reduces to one-dimensional resonant tunneling, and crosstalk will be prohibited. This situation is achieved by requiring simple symmetries in the waveguide and resonant modes, as shown in fig.2.6.

Here, the solid-line waveguide modes only couple with the solid-line resonant cavity modes, and similarly for the dashed-line modes. Essentially, there are three requirements that must be met:

- The waveguides must have mirror symmetry about their axis, and they must be single-mode in the frequency range of interest. (This mode will be either even or odd.)
- The resonant cavity in the center of the intersection, which governs coupling between the waveguides, must respect the mirror planes of both waveguides.
- In the frequency range of interest, the resonant modes must be odd with respect to one waveguide and even with respect to the other.

All three of these conditions are easily achieved. (In particular, the third condition is automatic for degenerate modes in intersections with sufficient symmetry [the symmetry group of the square].) The resulting transmission profile will be the typical spectrum of resonant tunneling--a Lorentzian (bell-shaped) curve centered on the resonance frequency. The width of the resonance is inversely proportional to the quality factor Q of the resonant mode (Q is proportional to the decay lifetime).

CHAPTER 3

FUNDAMENTALS OF OPTICAL PROPERTIES

In the world of Physics, the laws that govern the behavior of light are true to their nature. Among the several that exist, one is the law that describes Reflectivity, Absorptivity and Transmissivity. Consider a crystal as shown below with a ray of light incident on it normally from the top by a source of light.

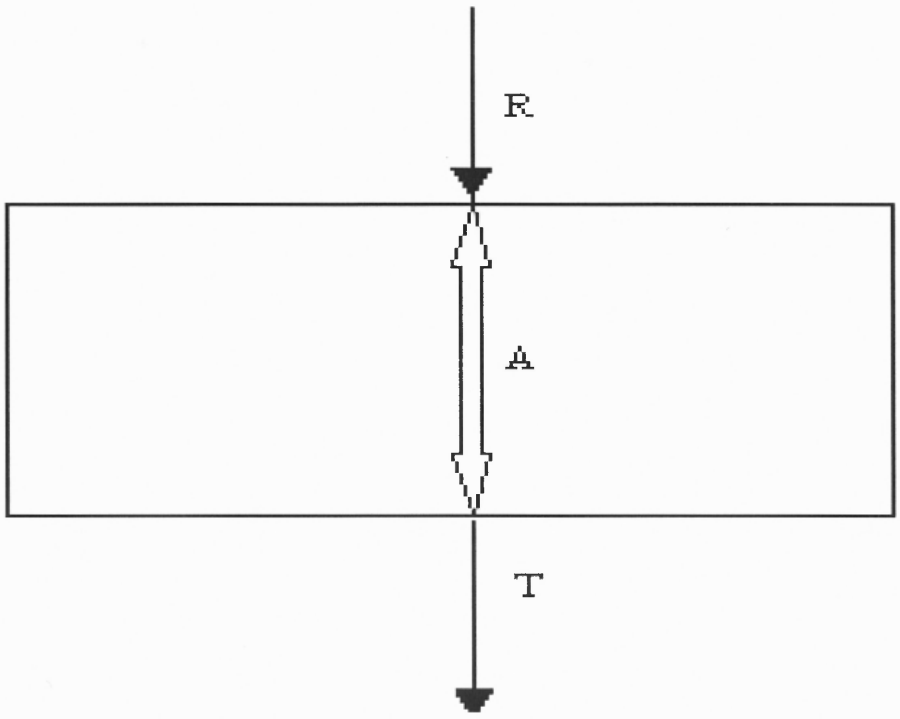

Figure 3.1 Reflection, Transmission and Absorption caused when a ray of light is incident on a crystal

As seen from the above figure, when a ray of light is incident on a slab of material, part of it is reflected back, a part of it is absorbed and the rest is transmitted through the material. In general such an event is governed by the equation

$$A(\lambda) + R(\lambda) + T(\lambda) = 1 \qquad (3.1)$$

Here 'R' is the reflectance, 'T' is the transmittance and 'A' is the absorptance of the material under consideration.

3.1 Reflectance, Absorptance and Transmittance of Radiation

These are the three main properties that are of concern in the domain of optics. They can be described in a number of ways.

3.1.1 Reflectance

It is an abrupt change in the direction of propagation of a wave that strikes the boundary between different media. At least part of the oncoming wave disturbance remains in the same medium. Regular reflection, which follows a simple law, occurs at plane boundaries. The angle between the direction of motion of the oncoming wave and a perpendicular to the reflecting surface (angle of incidence) is equal to the angle between the direction of motion of the reflected wave and a perpendicular (angle of reflection). Reflection at rough, or irregular, boundary will cause the ray to diffuse. The reflectivity of a surface material is the fraction of energy of the incoming wave that is reflected by it.

3.1.2 Absorptance

In wave motion, transfer of energy from wave to matter occurs as the wave passes through it. The energy of an acoustic, electromagnetic, or other wave is proportional to

the square of its amplitude--i.e. the maximum displacement or movement of a point on the wave; and, as the wave passes through a substance, its amplitude steadily decreases. If there is only a small fractional absorption of energy, the medium is said to be transparent to that particular radiation, but, if all the energy is lost, the medium is said to be opaque. All known transparent substances show absorption to some extent. For instance, the ocean appears to be transparent to sunlight near the surface, but it becomes opaque with depth. As radiation passes through matter, it is absorbed to an extent depending on the nature of the substance and its thickness. A homogeneous substance of a given thickness may be thought of as consisting of a number of equally thin layers. Each layer will absorb the same fraction of the energy that reaches it. The change in energy as the wave passes through a layer is a constant for a material for a given wavelength and is called its absorption coefficient.

3.1.3 Transmittance

In wave motion, transfer of wave energy through the material occurs i.e., it is the energy that can be seen emerging from the material when some sort of radiation is incident on it. Now consider the case when the material surface on which the ray is incident is not as smooth as above, but is now rough. In this case the above equation changes slightly to accommodate an effect called diffusion or scattering of light at the surface of the material.

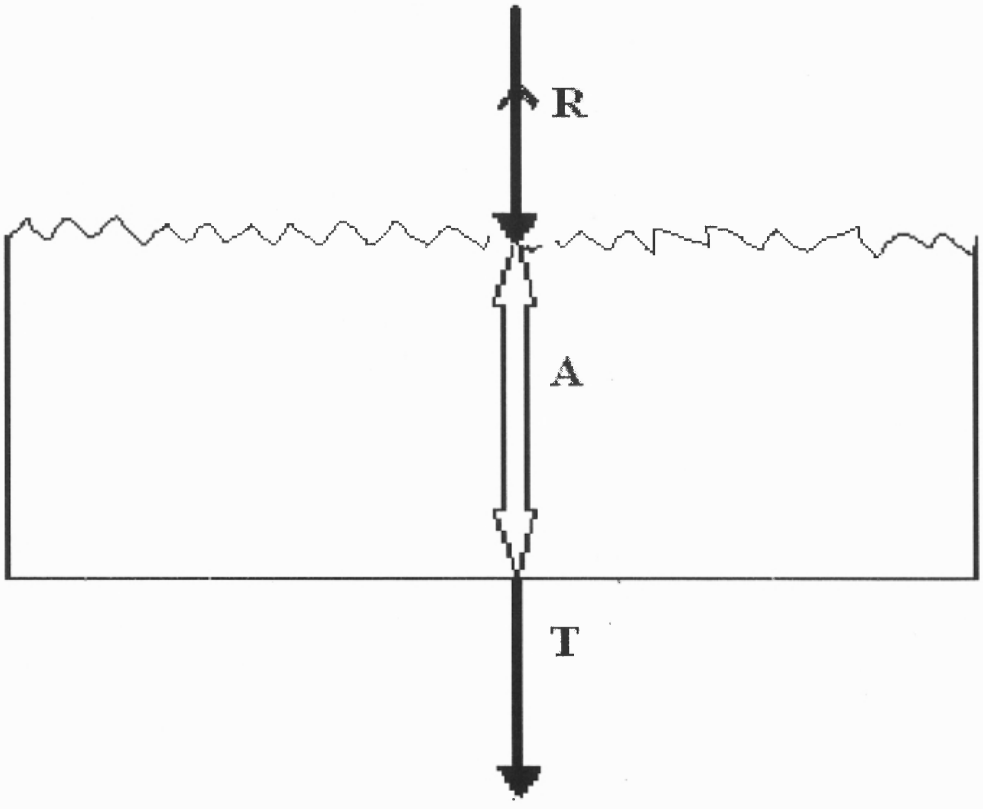

Figure 3.2 Reflection, Absorption and Transmission in case of radiation falling on a rough surface

The equation is now given by:

$$\mathbf{A^*(\lambda) + R^*(\lambda) + T^*(\lambda) = 1} \qquad \mathbf{(3.2)}$$

Here 'A*' is the apparent absorptance in the material under consideration and 'R*' and 'T*' are the apparent reflectance and apparent transmittance respectively. Now as one can see, it would not be possible to exactly predict the behavior of radiation at the surface of the material. Also, as a consequence of the roughness the surface area has increased. Therefore an apparent factor is brought into the picture. As the apparent absorption increases, the apparent reflection decreases.

3.2 Control of Properties of Materials

Many of the breakthroughs in today's world have resulted only after a deeper understanding of the properties of materials. Man was not satisfied with whatever material that he extracted in raw form from the earth. So he started tinkering with the existing materials to produce materials with even more desirable properties - from the luster of early bronze alloys to the reliability of modern steel and concrete. Today there is a collection of wholly artificial materials with a tremendous range of mechanical properties, thanks to advances in metallurgy, ceramics, and plastics. In the last decade a new frontier has emerged with a similar goal: to control the optical properties of materials. If materials that prohibit the propagation of light can be engineered, to allow it only in certain directions at certain frequencies, or localize light in specific areas, there could benefit enormously.

Next, there is a need to find such a material that can afford us complete control of light propagation. In this respect there is an analogy with successful and known electronic materials. A crystal is a periodic arrangement of atoms or molecules. A crystal lattice results when a small, basic building block of atoms or molecules is repeated in space. The geometry of a crystal therefore dictates many of the conduction properties of the crystal. In particular, the lattice might introduce gaps into the energy band structure of the crystal, so those electrons are forbidden to propagate with certain energies in specific directions.

The optical analogy is the *photonic* crystal, in which the periodic potential is due to lattice of macroscopic dielectric media instead of atoms. If the dielectric constants of the materials in the crystal are different enough, and the absorption of light by the material is minimal, then scattering at the interfaces can produce many of the same

phenomena for photons as the atomic potential does for electrons. The photonic crystal, which is a low-loss periodic dielectric medium, is thus one such medium, which can be optically controlled and manipulated. The concept of photonic crystals is pretty similar to that of metallic waveguides and dielectric mirrors. A metallic cavity does not allow electromagnetic waves to propagate below a certain threshold frequency, while a metallic waveguide only allows propagation along its axis. In this respect, photonic crystals can not only mimic the properties of cavities and waveguides, but are also scalable and applicable to a wider range of frequencies.

3.3 Fundamentals of Photonic Crystals

Spontaneous emission of light is a major natural phenomenon that is important in the world of Optics[10]. Take for example, LEDs, in which spontaneous emission fundamentally determines the maximum available output voltage. If the spontaneous emission of light can be controlled, this can mean major implications for optoelectronics and optical communications technology. The easiest way to understand the effect of a photonic band gap on spontaneous emission is to consider the following equation illustrated by figure 3. 3.

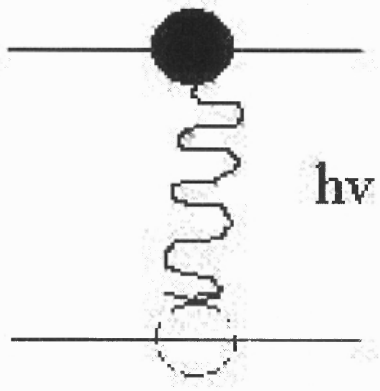

Figure 3.3 Spontaneous-emission event from a filled upper level to an empty lower level[10]

The downward transition rate ω between the filled and empty atomic levels is given by:

$$\omega = [\, 2\pi \mid V \mid^2 \rho\,(E)\,] / h \qquad (3.3)$$

where, |V| is sometimes called the zero-point Rabi matrix element and ρ(E) is the density of the final states per unit energy. In spontaneous emission, the density of final states is the density of optical modes available to the photon emitted in figure 3.3.

Metallic waveguides have a problem in the sense that they do not scale well into optical frequencies, as the metals become more and more lossy at these frequencies. Instead, if these materials are arrayed into a three-dimensionally periodic dielectric structure, a photonic bandgap should be possible. Its benefits are illustrated in figure 3.4.

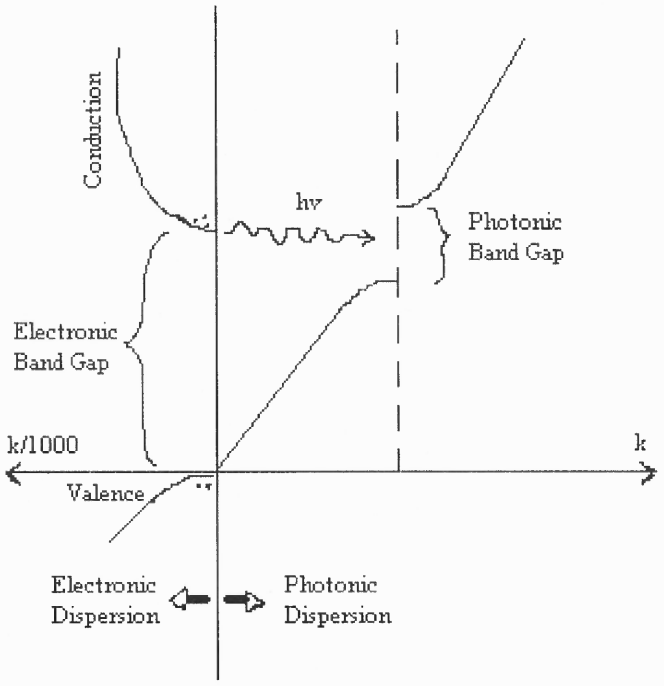

Figure 3.4 Right-hand side, the electromagnetic dispersion forbidden gap at the wave vector of the periodicity. Left-hand side, the electron wave dispersion typical of a direct-gap semiconductor[10]

In the above figure 3.4, the dots represent electrons and holes. Since the photonic band gap straddles the electronic band edge, electron hole recombination into photons is inhibited. The photons have no place to go[10]. One of the most important applications of this spontaneous emission inhibition is the enhancement of photon-number-state squeezing, which plays an important role in quantum optics.

The conventional method to convert optical energy into electrical signals could be described as follows. Effective photovoltaic material must absorb light to generate a mobile charge and to move that charge by means of a built-in electric potential. It was discovered in the 1830s that exposing an electrolytic cell to light increased the amount of

current it generated. But the first commercial Photovoltaic (PV) products arrived only in the 1950s, after silicon PV devices produced electricity with an efficiency of 4.5 percent. By 1960, the efficiencies of research devices reached 14 percent and commercial products attained 10 percent.

The simplest PV cell starts out as a wafer of crystalline silicon, in which each atom forms covalent bonds with four adjacent atoms in a highly ordered lattice. A potential is obtained by doping the silicon with boron and phosphorus. When boron, with three valence electrons, bonds at a site normally occupied by a silicon atom, with four, one bond must accept an electron from the crystal lattice. Left behind is a positively charged mobile carrier (or hole) that leads to p-type material.

Phosphorus, with five valence electrons, donates an electron to the lattice to create an n-type material. The ionized impurity is fixed in the silicon crystal lattice, which contains a balancing number of mobile electric charge-carriers of opposite charge. Normally, Boron is contained in the wafers used for PV cells in minute, part-per-million concentrations. As for the phosphorous, a high-temperature process diffuses it into the wafer surface in slightly greater concentration than the boron background. The junction between n-type and p-type material drives all the mobile charge from the region, leaving a built-in potential sustained by the fixed ionized acceptors and donors. When the silicon absorbs a photon, the event frees an electron to become a mobile carrier and simultaneously creates a hole. The p-n junction, with its built-in electric field, can separate the electron and hole, and the current thus generated can flow when the device is connected to an external circuit as shown in figure 3.5. Device efficiency is defined as the

ratio of the electric power produced to the power of the incident light, or the total number of photons. In the modern era, there are very few methods that work efficiently inorder to

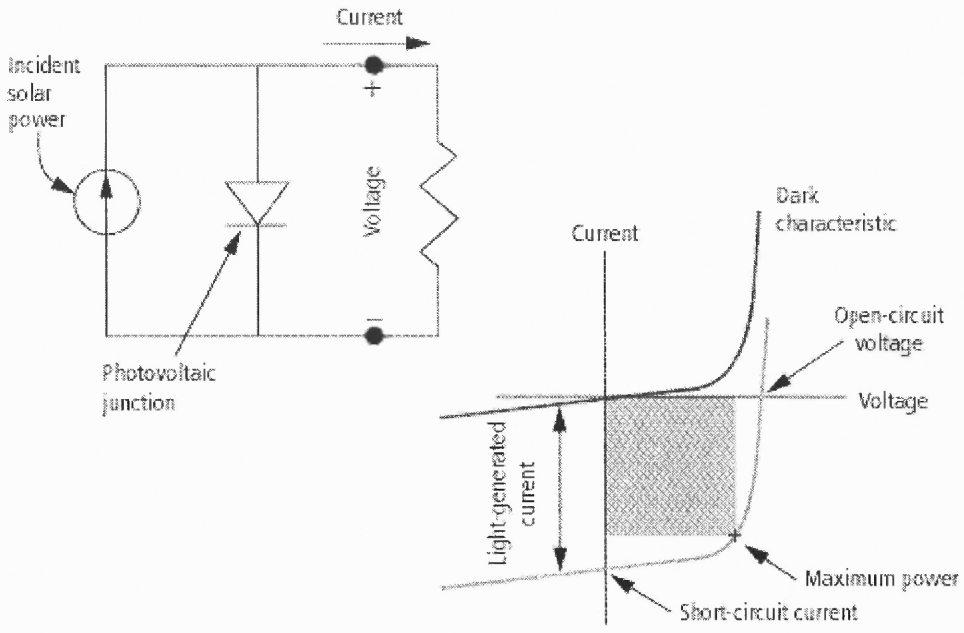

Figure 3.5 A photovoltaic diode[29]

optical energy into electrical energy. One of the most recent methods is described next. Virginia Tech researchers[30] from various departments are working with a local company to create thin films that convert light into electricity. These scientists are using the ionically self-assembled monolayers (ISAM) process to fabricate optoelectronic devices. The process allows molecule-thick layers of oppositely charged materials to build up on a base structure.

In this case, one of the layers is made up of carbon molecules known as Fullerenes and another layer is a positively charged polymer. Fullerenes have high electron affinity, so they will accept electrons easily from photoexcited molecules of a conducting polymer, creating a polymer with a negative charge. The result is a material to

be used in a solar cell, generating a current from a negatively charged Fullerene and a positively charged polymer. Thus a photovoltaic device is created without the use of toxic solvents or expensive instruments and under ambient conditions[38].

CHAPTER 4

MODELING OF OPTICAL PROPERTIES

The modeling of optical properties of the samples used in the course of this research was performed using a PC-based software called Multi-Rad. This software is capable of calculating the optical properties of thin-film stacks, with emphasis on silicon related materials and structures.

4.1 Multirad

4.1.1 Introduction to the software

At the heart of the calculations is thin film optics, implemented in the form of the matrix method of multilayers[21]. This model assumes that the layers are optically smooth and parallel, and the materials are optically isotropic (the optical constants are not dependent on crystallographic orientation). Therefore, the theory does not predict any variation of properties in the azimuthal direction. For a given multilayer stack at a prescribed temperature, the user can calculate the optical properties as they vary with wavelength and angle of incidence.

4.1.2 Spectral Analysis

The program assumes that there is no variation in properties over the azimuthal angle (or angles) of incidence that are being considered[21].

4.1.3 Spectral Range

The spectral range over which the properties can be calculated, varies from 0.4 to 20 μm and the calculation can be performed in increments of 0.001μm. The smaller the increment, the more the calculated data points, and it would take longer to do the calculation.

4.1.4 Stack Information

As many as up to 100 layers can be defined in this software. The light will be incident on layer #1 and measurements will be carried out on the basis of the light transmitted from the same layer. We can add each layer by scrolling through the list of materials that can be added. In addition to defining each layer, its doping concentration, thickness and process temperature can be specified. The version of Multirad used here allows only the optical constants of silicon to be temperature dependent, so the temperature of all other materials in the stack has no effect on the result. The model for the optical constants of silicon is based on the work of Hebb and Jensen[22]. The simulation can handle temperature variations from 30 to 1400 °C (melting point of Si).

4.1.5 Calculation

Once the angle of incidence, spectral range temperature and stack are defined, the program can be run and it will simulate the optical behavior of the stack of layer as specified by the user.

.

4.2 Calculating Optical Properties of Thin Film Stacks

4.2.1 Spectral Directional Optical Properties

Optical properties of the wafer and other surfaces in the enclosure are calculated using the matrix method of multilayers[21, 23]. This method predicts the reflectance and transmittance of a multilayer stack for a given wavelength and angle of incidence. Radiation at a given wavelength is treated as coherent, so interference effects are taken into account. The main assumptions of the theory are that the layers are parallel and optically isotropic, the surface is optically smooth, and the area in question is much larger than the wavelength of incident radiation (no edge effects).

4.2.2 Integrating Over Angle of Incidence

To obtain the hemispherical spectral properties, integration over all directions in the hemisphere is performed.

4.2.3 Integrating Over Wavelength

To calculate the total amount of energy that will be reflected, transmitted, emitted or absorbed in a certain spectral range, the spectral properties must be integrated with respect to wavelength for a blackbody distribution of energy.

4.2.4 Application to Pyrometry

Multirad can be utilized for applications in pyrometry. A change in emittance of a multilayer stack at a given nominal temperature difference leads to pyrometric temperature error. A rigorous calculation of this error must take into account the pyrometer, the associated optics, filters, and many other complicated factors, which are

beyond the scope of MultiRad. The software, though, does give a calculation of this error to yield an estimate of the impact of uncertainty in layer thickness on temperature measurement error. The following expression provides this estimate[24]

$$\Delta T = \frac{T^2_{nom}\lambda \ \Delta\varepsilon}{14400 \ \ \varepsilon} \tag{4.1}$$

where, T_{nom} is the nominal wafer temperature that would be measured if the stack has the nominal emissivity, ε, $\Delta\varepsilon$ is the emissivity of the stack due to a change in the film thickness of one or more layers in the stack, and ΔT is the temperature measurement error incurred due to this emissivity change.

4.3 Optical Constants of Materials

4.3.1 Single Crystal Silicon and Polysilicon

The spectral dopant concentration and the temperature ranges, which are relevant for Rapid Thermal Processing (RTP) must be defined in order to construct a dielectric function model for a single crystal silicon. In order to have greater accuracy, the dielectric function model, should be valid for wavelengths as small as 0.4μm. The model should also be valid for active carrier concentrations greater than 10^{20} cm^{-3}, which can be achieved through annealing of shallow heavy dose implants. Finally, the frequency of radiation ω, the temperature of silicon T, N_D the donor dopant concentration, N_A the acceptor concentration, n and k the refractive index and extinction coefficient, need to be known respectively, in order to calculate the dielectric function for single crystal silicon. In order to calculate the extinction coefficient for wavelengths between 0.4 and 0.9μm, the semi-empirical correlation proposed by Jellison and Modine[25] can be used.

For wavelengths greater than 0.9μm, the contribution of the dielectric function for absorption by interband transitions is taken into account by using the model of Timmans[26], which is based on the model of Macfarlane et al.[27]. This model also accounts for phonon assisted indirect transitions across the band gap, including the effects of temperature dependence of the band gap. The refractive index is not affected by the absorption caused by lattice vibrations, which are relatively weak[28]. For wavelength ranges between 0.8 and 10μm, the correlation given by Magunov[29], which is valid at temperatures up to 1400K, is used. The contributions to the dielectric function by carrier absorption of electrons and holes is given by the semiclassical Drude Theory[30]. The number of thermally generated carriers is calculated by the expressions given by Thurmond[31]. To evaluate the temperature dependent electron and hole scattering mobilities from the measurements of Morin and Maita[32] for temperatures up to 1100K, the data of Strum and Reaves is used for wavelengths of 1.55 to 3.4μm[33]. The data of Strum and Reaves was extracted from high temperature transmission measurements at two laser wavelengths in a lamp based Rapid Thermal Processing (RTP) system. The data of Timmans was extracted from high temperature emittance measurements using an electron beam based RTP system.

4.4 Limitations

Multirad does have certain limitations in its ability to perform simulations. Some of the assumptions made in it are listed below:

a. It considers an abrupt interface.

b. It does not consider the effects of roughness.

c. It considers only Silicon as the substrate material and hence the free carrier absorption depends only on silicon.

d. It neglects the temperature dependence of optical properties of all layers except silicon.

CHAPTER 5

EXPERIMENTAL APPROACH

5.1 Bench top Emissometer-Description of the Apparatus

A spectral emissometer has been used to measure the optical properties of the materials that have been investigated in this study. The Bench top Spectral Emissometer measures the radiative properties of a sample over a wide spectral range, in the near and mid-infrared, from 12500cm^{-1} to 500 cm^{-1} (0.8 to 20 μm). The schematic of the Bench top Spectral Emissometer is shown in figure 5.1. It consists of a hemi-ellipsoidal mirror having two foci, both inside the mirror. At one focus, the exciting source, which is a black body, is placed and the sample under investigation is placed at the other focus.

A microprocessor controlled motorized chopper facilitates in simultaneous measurement of the sample spectral properties such as radiance, reflectance and transmittance. A carefully adjusted set of five mirrors provides the optical path for the measurement of the optical properties. An oxy-acetylene/propane torch provides the source of heating of the samples. The sample size is typically in the range of 0.5 to 1 inch in diameter. Thus the temperature estimation, using the emissometer, is assumed to be uniform over this small region of the sample. However, because of safety considerations and potential sample contamination, various alternatives to heat the samples, uniformly in a controlled environment, are being investigated.

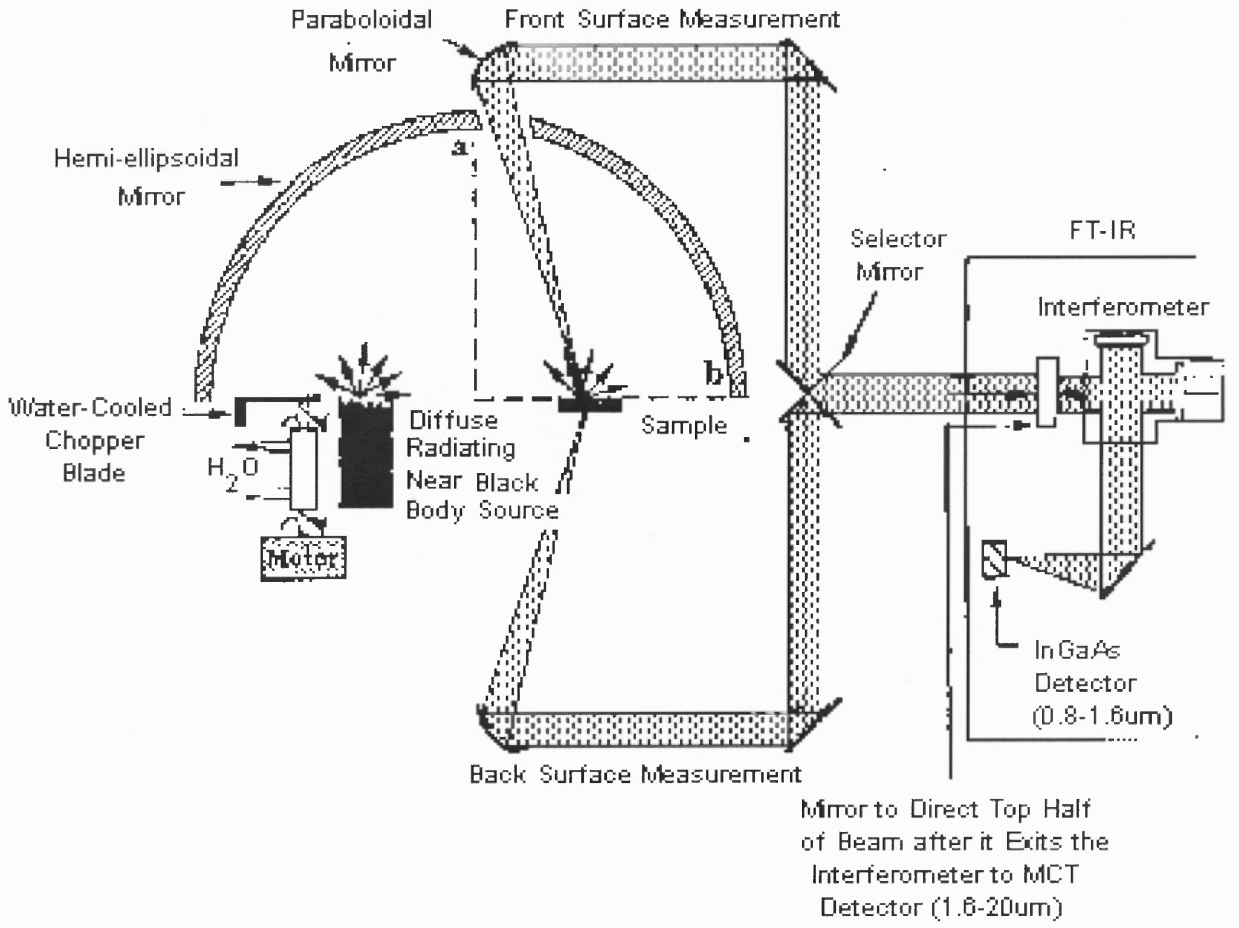

Figure 5.1 Schematic of bench top emissometer showing components and optical paths for radiance, reflectance, and transmittance measurements

The spectral emissometer consists of three GaAs lasers to facilitate in aligning the sample at the appropriate focus. A high resolution Bomem FTIR spectrometer, consisting of Ge and HgCdTe detectors, interfaced with a Pentium processor, permits data acquisition of the measured optical properties. Fourier Transform Infrared (FTIR) Spectroscopy involves a special mathematical treatment of the experimentally measured spectral data[35]. Markham et.al.[36] have designed and constructed a bench top FTIR instrument which allows for measurement of radiance, directional-hemispherical reflectance and directional hemispherical transmittance of materials at elevated temperatures from 50 to 1000 °C over a wide spectral range from 12500 to 500 cm^{-1} (0.8 to 20 μm).

The on-line computer enables the user to flip the mirror to acquire transmission/reflection via software configurations such as Spectra Calc and GRAMS. This instrument has many applications, namely: (1) industrial quality control of radiative properties of processed materials, (2) research and development of new materials and temperature measurements by optical techniques in the near and mid IR ranges.

5.2 Methodology of Emissometer

The spectral emissometer allows simultaneous measurements of radiance R, reflectance ρ, transmittance τ and the temperature T of the sample at the measured point. The theoretical background and methodology is as follows[37]. A sample is placed at one of the foci of the hemispherical ellipsoidal mirror while the source, a blackbody at 900 °C, is at the other focus. The chopper (in figure 5.1) permits the simultaneous acquisition of the

radiative properties of interest including the sample temperature. A front-surface sample measurement, with the chopper closed, yields the sample's directional spectral radiance, which is given by:

$$\mathbf{R_\nu\,(T) = \varepsilon_\nu\,(T)\,R_\nu^{\,b}\,(T)} \qquad \mathbf{(5.1)}$$

where, ε_ν (T) is the emissivity of the sample at temperature T and $R_\nu^{\,b}$(T) is the theoretical Planck function at temperature T. The subscript ν denotes the spectral frequency.

When the chopper is open, the measured radiation M_o will include that emitted by the sample and the blackbody source radiation reflected by the sample in spectral directional hemispherical mode:

$$\mathbf{M_o = R_\nu\,(T) + \rho_\nu\,(T)\,R_\nu^{\,b}\,(T_{bb})} \qquad \mathbf{(5.2)}$$

where, T_{bb} Is the constant blackbody source temperature, which is maintained at 900 °C and ρ_ν is the spectral directional-hemispherical reflectivity. The difference in the two measurements is thus q_ν (T) $R_\nu^{\,b}$ (T_{bb}). The constant source radiation $R_\nu^{\,b}$ (T_{bb}) is quantified by replacing the sample with a perfect reflector (a gold mirror, $q_\nu^{gold} \sim 1.0$) and measuring the spectrum in the chopper open condition. Thus, the directional-hemispherical reflectance of the sample, ρ_ν (T), can be determined.

For an opaque sample, the spectral emittance, $\varepsilon_\nu = 1-\rho_\nu$. Using the equation $R_\nu^{\,b}$ (T) = R_ν (T)/ ε_ν (T), the surface temperature of the sample can be determined by direct integration over the entire region:

$$\mathbf{\int R_\nu^{\,b}\,(T)\,d\nu = \sigma\,T^4} \qquad \mathbf{(5.3)}$$

where, Stefan Boltzmann constant $\sigma = 5.67 * 10^{-12}$ W cm^{-2} K^{-4}. The sample temperature can be obtained to within ± 10 °C. For non-opaque samples, the directional-hemispherical transmittance, τ_ν is measured by flipping the selector mirror and measuring the back

surface radiance plus transmittance. The source radiation is quantified with the sample absent, and the analysis to determine τ_v follows that for ρ_v. The more extensive closure relationship $\varepsilon_v = 1-\rho_v -\tau_v$ is then used to determine ε_v. The temperature of the samples can also be determined simultaneously by fitting the sample's radiance to the Planck's blackbody curves.

5.3 Experimental Details

The samples used in all measurements are fabricated by using a layer-by-layer design because of the relative ease of construction[7]. The structure consists of layers of one-dimensional rods with a stacking sequence that repeats itself every 4 layers. Within each layer, the rods are parallel to each other and have a fixed pitch. The orientation of the rods on alternate layers is rotated 90° between the layers. Between every 2 layers, the rods are shifted relative to each other by an amount equal to half the pitch between the rods. The resulting structure has a face-centered-tetragonal lattice symmetry, of which a face-centered cubic is a special case. The crystals are formed by the use of advanced silicon microelectromechanical systems and integrated circuit processes. The approach relies on the fact that when a thin film of material is deposited over a step and then subjected to anisotropic reactive-ion etching, a thin sliver of material remains along the sides of the step. If the step height is several times greater than the thickness of the thin film that is deposited, then the width of the fillet will be identical or at least proportional to the film thickness.

The final structure of the 3D crystal is obtained by use of advanced silicon microelectromechanical systems and circuit processes as summarized by Fig. 5.2. In the first step of the process [Fig. 5.2(a)], a thin film of polysilicon of thickness 0.22 μm is deposited on the substrate. The polysilicon is then capped with a thin film of silicon nitride that acts as a combination etch and chemical mechanical polish (CMP) stop. The sacrificial step material is then deposited. A plasma-enhanced silicon dioxide is used in this step. The layer is then photopatterned as shown in Fig. 5.2(b). After photopatterning, the oxide is anisotropically etched to just above the level of the silicon nitride layer.

A 30-s wet etch in a room temperature 6:1 mixture (ammonium fluoride: hydrofluoric acid) is then used to isotropically remove about 90nm of silicon dioxide as shown in Fig. 5.2(c). This is done to ensure that the silicon nitride is exposed and to relax slightly the minimum feature requirement of photolithography. Polysilicon is used to form the fillet as in Fig. 5.2(d). The polysilicon is then etched in a high-density plasma-source system as in Fig. 5.2(e). After fillet formation, the sacrificial oxide is tripped as in Fig. 5.2(f). The fillet is then used as a mask for etching of both the underlying silicon nitride and silicon dioxide layers as in Fig. 5.2(g) and (h). The next critical step in the processing involves the use of CMP to maintain planarity throughout the process. The first step is to fill the gaps between the line of polysilicon with a 0.3 μm deposition of silicon dioxide as seen in Fig. 5.2(i).

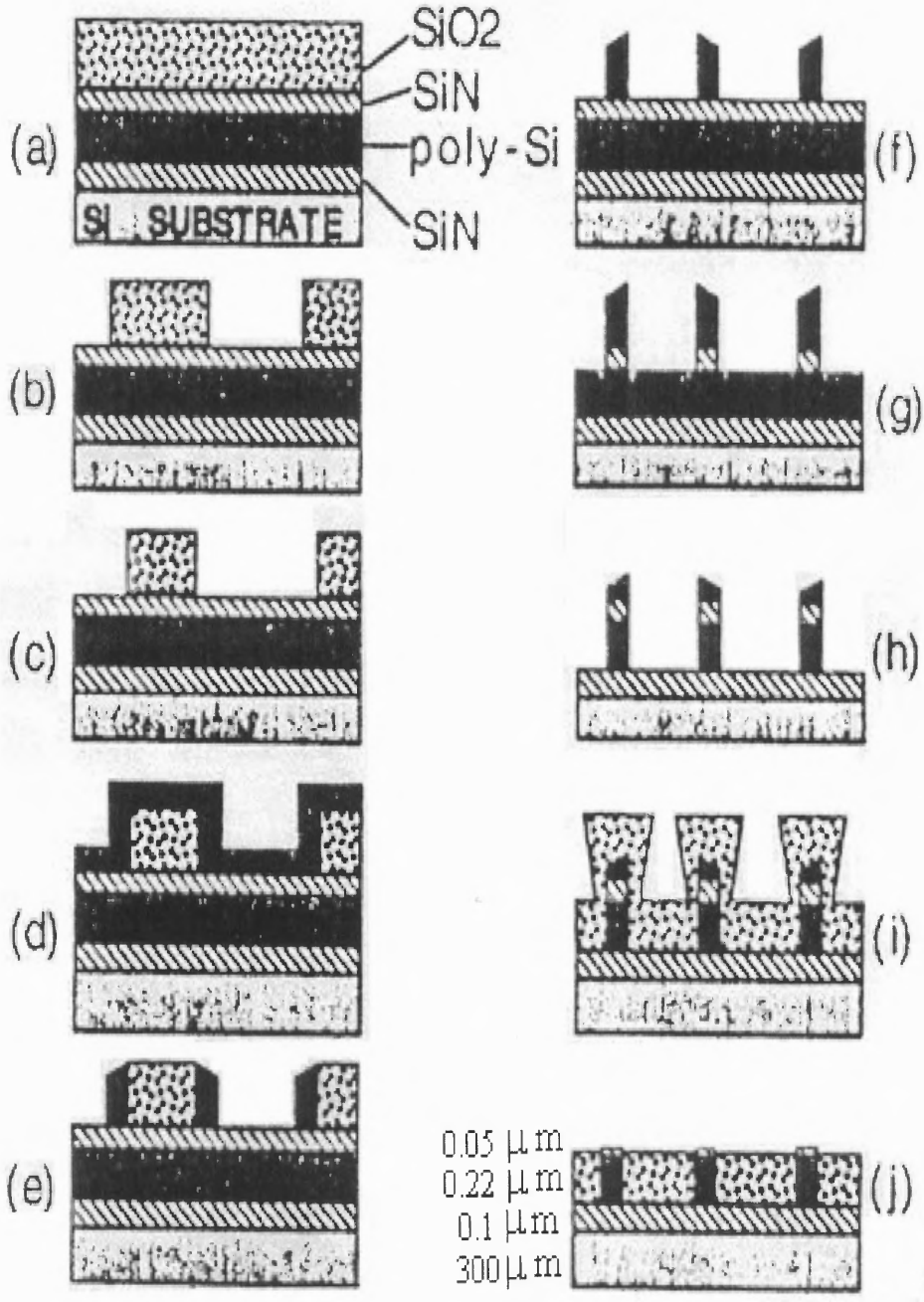

Figure 5.2 Schematic of the process flow used to produce a single level of the sample used for measurement of experimental data

The wafers are then planarized back to the silicon nitride-stopping layer by use of CMP as in Fig. 5.2(j). The entire process is then repeated to get the subsequent three or four layers of the structure. After completion of the desired number of layers, the silicon dioxide between the polysilicon lines is removed in a concentrated hydrofluoric acid-water solution with excellent selectivity between polysilicon and silicon dioxide.

CHAPTER 6

RESULTS AND DISCUSSION

6.1 Background

The optical properties of photonic crystals at room temperature have been studied extensively, partly because of its fundamental interest and importance as a medium that can trap light and partly because it is an important medium in optical communication. Fig. 6.1 and 6.2 represent schematics of optical communication system along with the sub components that comprise the system. Devices such as photonic crystals can be deployed between the driver and the laser and also between the laser and detector. The obvious intent is to improve a.) the electrical signal to optical signal (E/0)conversion efficiency and b.) Laser to wavelength match at the desired bandgap/optical absorption edge.

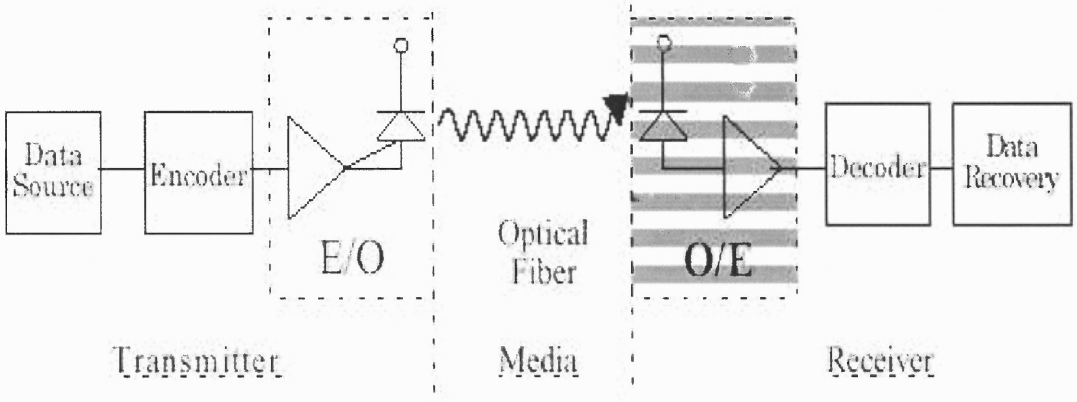

Fig. 6.1 Block Diagram of a typical optical data link[35]

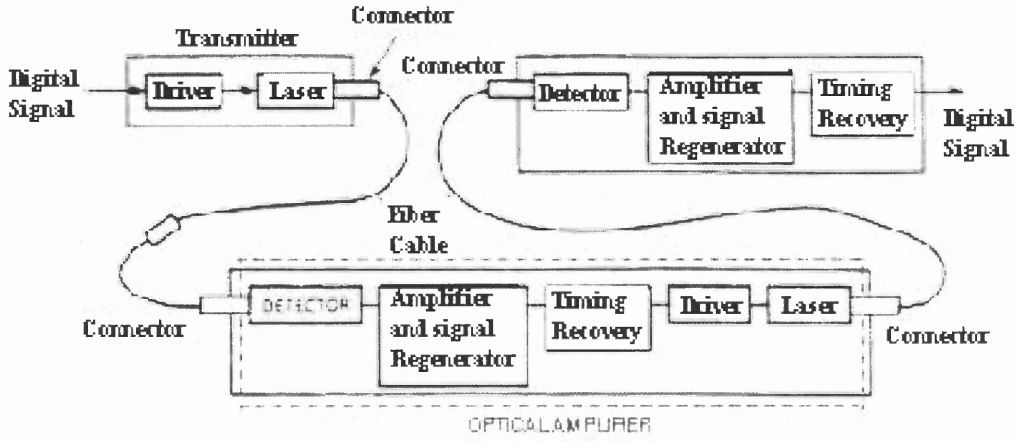

Fig 6.2 Block diagram showing different blocks in a optical transmission system[35]

In general, the low transmissivity, for the photonic crystal in the region of 1.3 to 1.5 μ is attributed to the presence of the "photonic bandgap" in that region. It is this characteristic of the photonic crystal that is being looked into in the discussion, so as to exploit the bandgap engineered structure for applications in lasers, filters, etc.

6.2 The Absorption Coefficient

Absorption coefficient is a measure of the attenuation caused by absorption of energy that results from its passage through a medium. Absorption coefficients are usually expressed in units of reciprocal distance. The absorption coefficient is related to the transmission by the equation as shown below:

$$dF = -b_a F\, dx \qquad \text{where } b_a \text{ is a constant.}$$

Integration would give $F(x_2) = F(x_1) \exp(-\delta_a)$

$$\delta_a = \int_{x1}^{x2} b_a x\, dx \qquad \text{where x1 and x2 are surfaces between which the ray travels.}$$

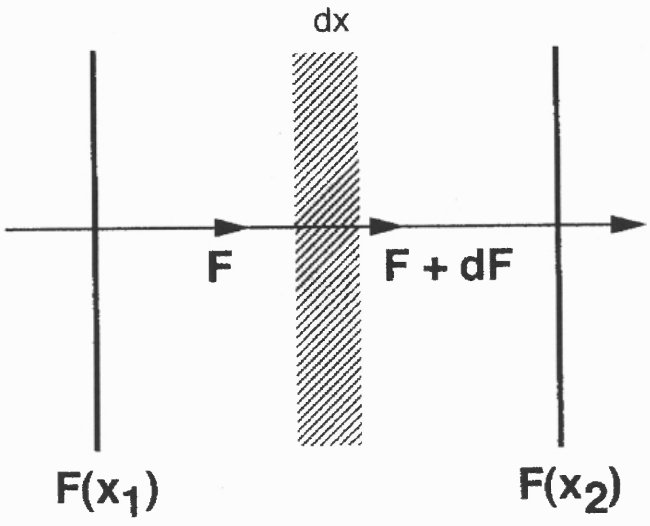

Fig 6.3 Transmittance through a medium

For homogenous medium: $b_a(x) = b_a$ independent of x

$F(x_2) = F(x_1) \exp[-ba\ (x_2-x_1)]$

$T = F(x_2)/F(x_1) = \exp(\delta_a)$ ----------transmittance

$\alpha = [F(x2)-F(x1)]/F(x1) = 1- T$----------absorptance

As can be seen from the above set of relations, there is a distinct relation between absorption coefficient of a medium and the transmittance through the medium. It is this relation which prompts us to study in more detail the behavior of light through a photonic crystal.

6.3 Effects on the Transmittance of Photonic Crystals

The transmittance of a photonic crystal is dependent on a number of factors, which can be seen from the experiments carried out on the samples. As the number of layers is increased, it is observed that the transmittance through the photonic crystal rapidly

decreases to a minimum in a certain range just as Flemming and Lin[7] have documented it. It can be seen from the graph in fig. 6.4 that, the transmission spectra differ by only a mere 15% (3L and 4L) or there is only a 15% layer-to-layer misalignment of the optical 3D crystal. This may be a result of defects in the crystal or due to misalignment between certain layers. In the present study, comparisons of the experimental results are made with results based on simulation shown in fig. 6.5. Because of the limitations of the 1-D simulation, two particular case studies considering the presence of (a) poly-Si as the significant layer and (b) SiO_2 as the significant layer are evaluated.

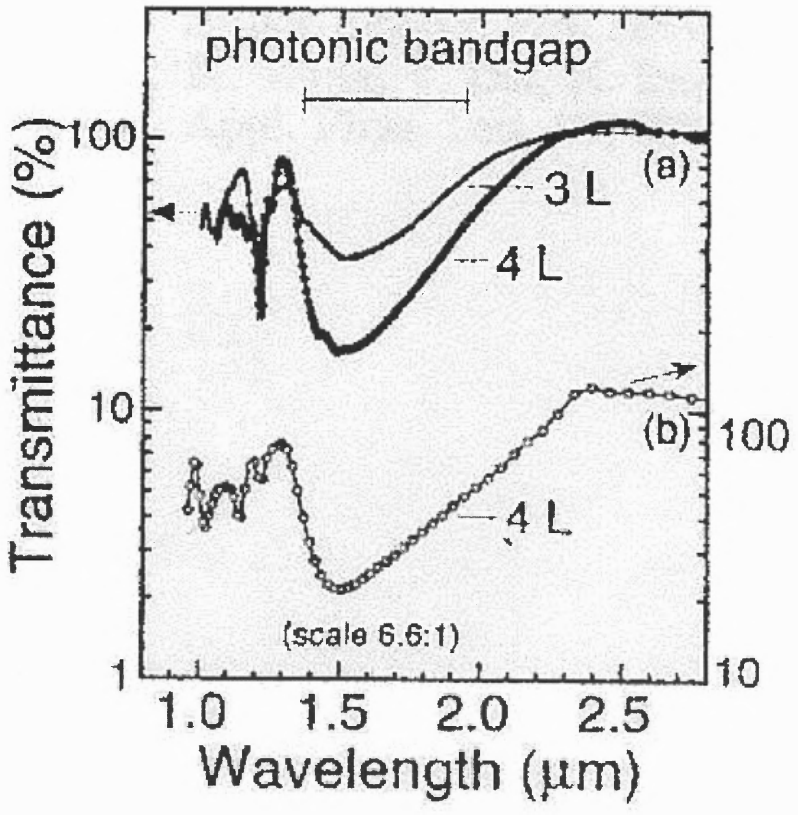

Figure 6.4 Transmission spectrum for the 3D optical photonic crystal. The wavelength axis is scaled with a ratio 6.6:1(Sandia)[7], 3L – three layers, 4L – four layers

In the above fig 6.4, the transmittance spectrum for a 3D photonic crystal is plotted on a logarithmic scale as a function of wavelength from 0.5 to 3.0μm. A strong transmittance dip is observed at λ=1.35 and it repeats at λ=1.5μm. This provides enough evidence of the existence of a photonic bandgap in the optical wavelengths. The gap extends over a spectral range of $\Delta\lambda$ = 0.6μm; the gap-midgap ratio of $\Delta\lambda/\lambda$ = 36% is large. The development of the bandgap is clearly evident as the number of overlayers is increased from three to four. At wavelength beyond 2.8μm, the transmission through the crystal saturates to 100%. For comparison purposes, a transmittance plot taken from an infrared 3D crystal is also shown by curve (b) in fig. 6.4. The design of the optical and the infrared 3D crystals is identical, except that their respective dimensions are different by a ratio of 6.6:1. The vertical axis is shifted downward by 10dB for ease of comparison. The details of the transmission spectra for both samples are identical, despite the ~15% layer-to-layer misalignment of the optical 3D crystal. This comparison verifies that, indeed, a photonic bandgap scales linearly with the device dimensions. It also shows that a layer-by-layer design is relatively insensitive to slight process instabilities. One possible reason for this is that, in this approach, defects do not tend to be cumulative.

6.4 Results of Simulation

Simulations were carried out using a software package from MIT called Multirad[23]. Multirad is capable of simulating the emittance, reflectance and transmittance spectra of various layers of silicon related materials and structures. Multirad requires data files that contain the wavelength dependent refractive indices and the extinction coefficient of materials, as input for simulation. There is of course the restriction that the simulation can

only be carried in one dimension as opposed to 3D wavelength, which would be ideal. In figs. 6.5 and 6.6, the plots of transmission versus wavelength obtained from simulation are shown. In the cross-section of the photonic crystal containing polysilicon as the significant layer, the transmittance of the photonic crystal has a lower minimum when compared to the cross-sections in which, it is silicon dioxide. This may point out to the fact that the cross-section with polysilicon layer as the significant layer is the more dominant of the two cross-sections. It can also be seen that the dip in transmittance in case 2(polysilicon) is in a broader wavelength range. In both cases, several dips are observed in the λ= 1.0 to 2.8μm region, meaning that there is a photonic bandgap in these wavelength range. Also, as the numbers of layers in the crystal are increased, the transmittance spectrum is more distinct.

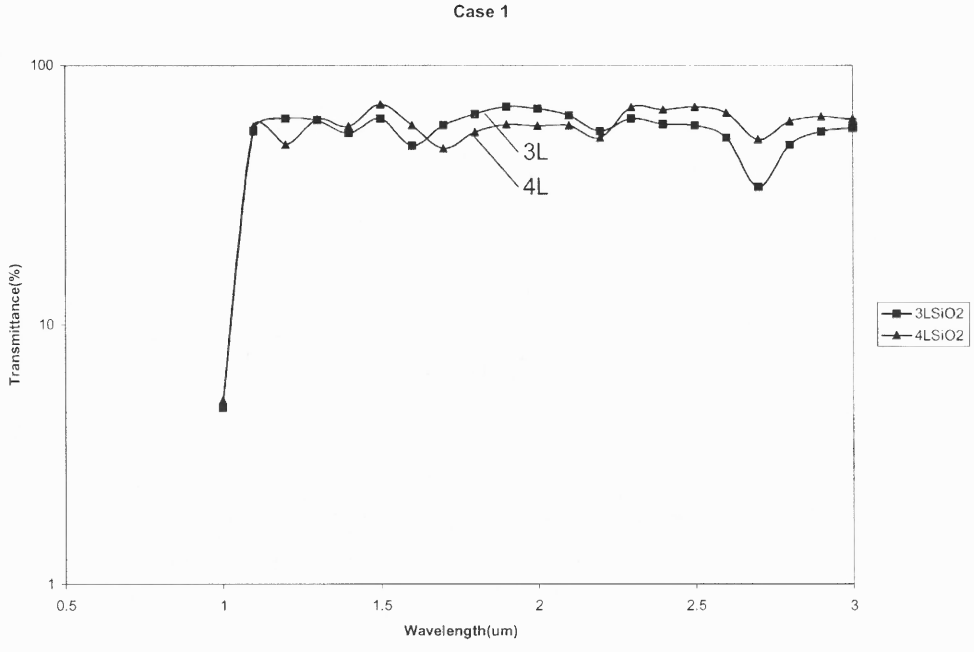

Fig 6.5 Simulated transmission spectrum for the 1D optical photonic crystal. The wavelength axis is scaled with a ratio 6.6:1(Cross section with SiO_2 as the significant layer)

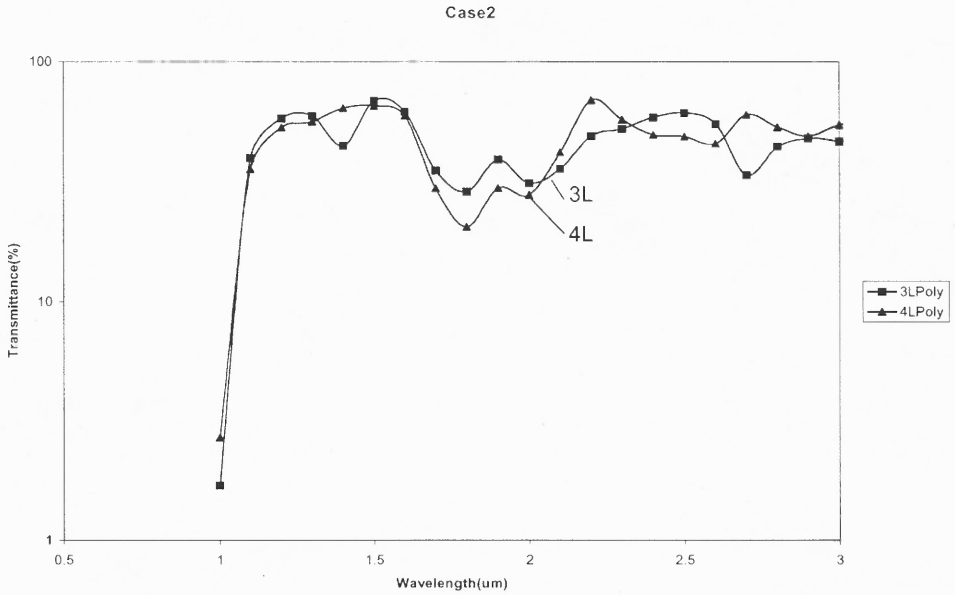

Fig 6.6 Simulated transmission spectra for the 1D optical photonic crystal. The wavelength axis is scaled with a ratio 6.6:1(Cross section with PolySilicon as significant layer)

6.5 Effects of Layers on the Photonic Crystal

As the number of layers is increased from one to three, it can be seen that there is some effect on the behavior of the crystal as a whole. Consider for example the response of a single layer crystal.

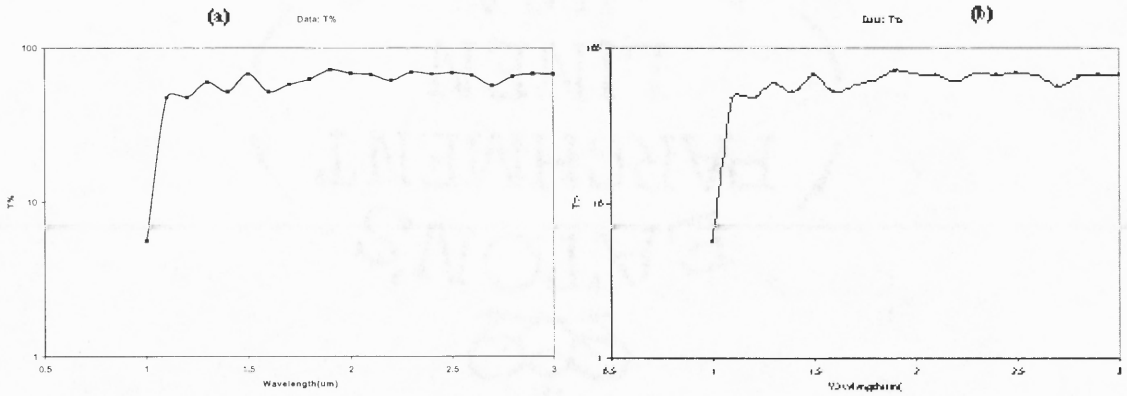

Figure 6.7 Simulated transmission spectra through a single layer of photonic crystal for cross-sections containing (a) SiO_2 and (b) Poly-Si as the significant layer

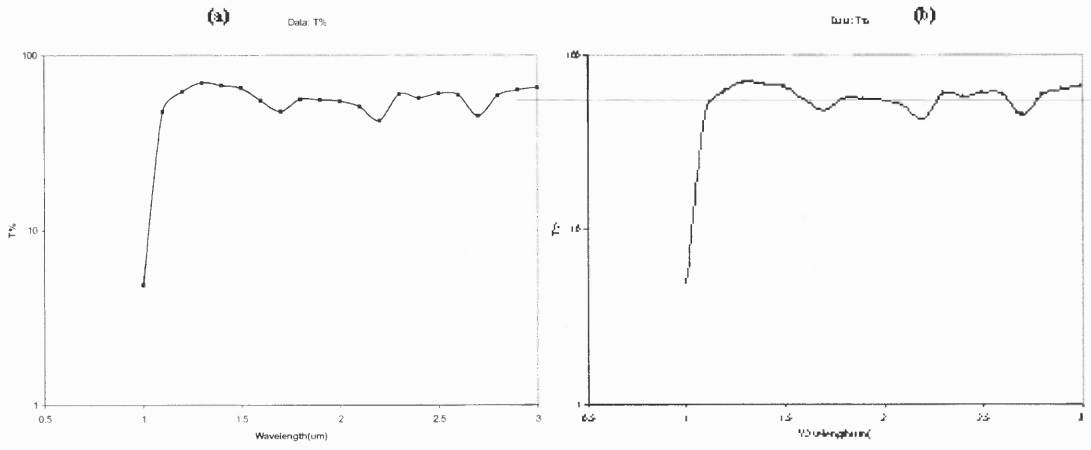

Figure 6.8 Simulated transmission through two layers of the photonic crystal for cross-sections containing (a) SiO_2 and (b) Poly-Si as the significant layer

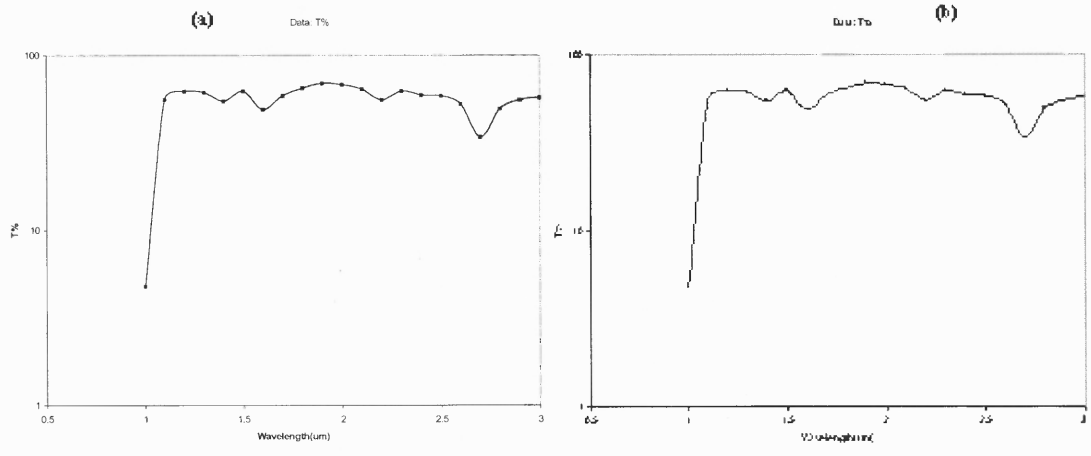

Figure 6.9 Simulated transmission through three layers of the photonic crystal for cross-sections containing (a) SiO_2 and (b) Poly-Si as the significant layer

As can seen in figs. 6.7, 6.8 and 6.9, the increase in the number of layers results in an increased variation in transmittance. It can be seen that the minima and maxima, become more pronounced, as each successive layer is added.

6.6 Effects Within Each Layer of the Photonic Crystal

As has been discussed in chapter 5, each layer in the photonic crystal is composed of sub-layers of material. It would thus be interesting to study the transmission spectra after the addition of each successive sub-layer in the crystal as it would give an idea as to how the various layers contribute to light trapping in the photonic crystal.

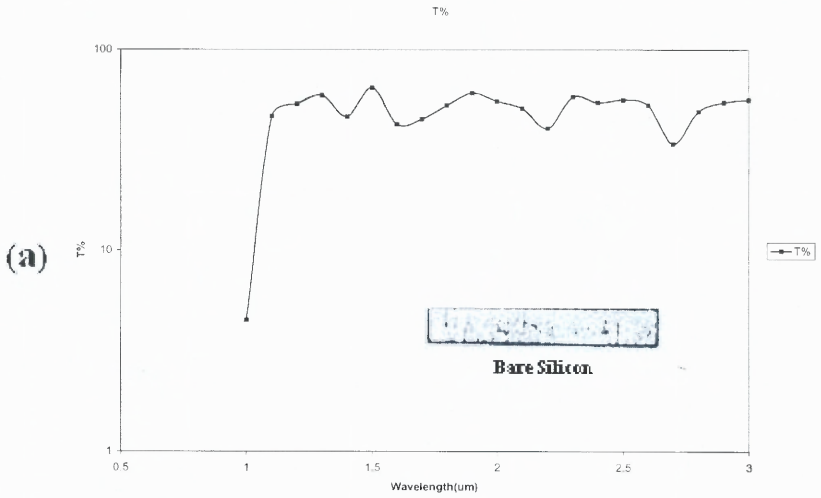

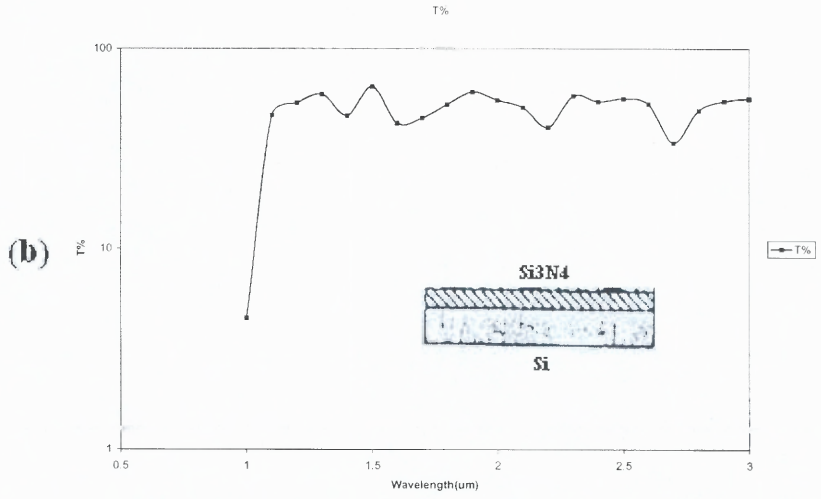

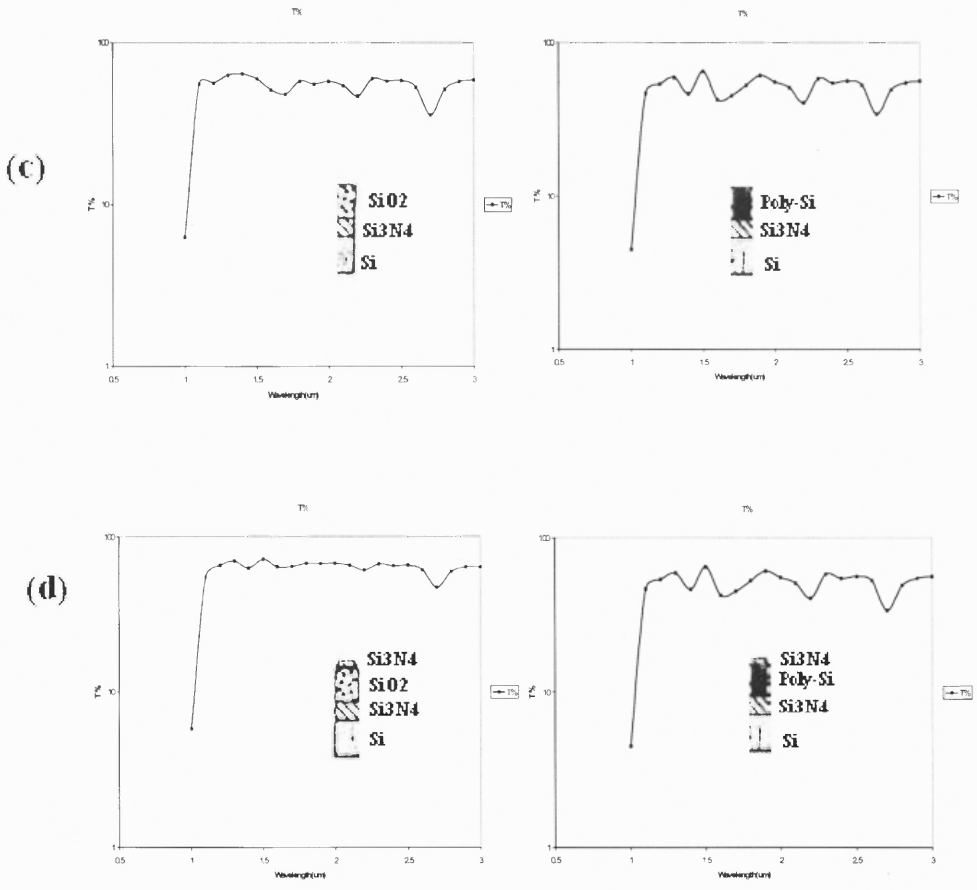

Fig 6.10 Transmission spectra for (a) Substrate only; (b) Si_3N_4/ Substrate; (c) SiO_2/ Si_3N_4/ Substrate (d) Transmission spectra for Si_3N_4/ SiO_2/ Si_3N_4/ Substrate (one layer)

The transmission spectra for various sub-layers in a single layer of the photonic crystal are shown in figs. 6.10 a-d. There is a pronounced aspect that can be noticed in all these spectra. With the addition of each sub-layer, the transmittance variations through the layer decrease. This is because of the addition of dielectric layers on silicon, which has the effect of dampening the variation in transmittance.

6.7 Experimental Data of Photonic Crystals

The results of transmittance of photonic crystals, with measurements taken independently on both the front and backside, using a spectral emissometer at room temperature are presented in figures 6.11(a) and (b) respectively. The sample used in these measurements is the one that has been previously described in chapter 4. The observed sharp rise in the transmittance at 1.1μm corresponds to the absorption edge of silicon.

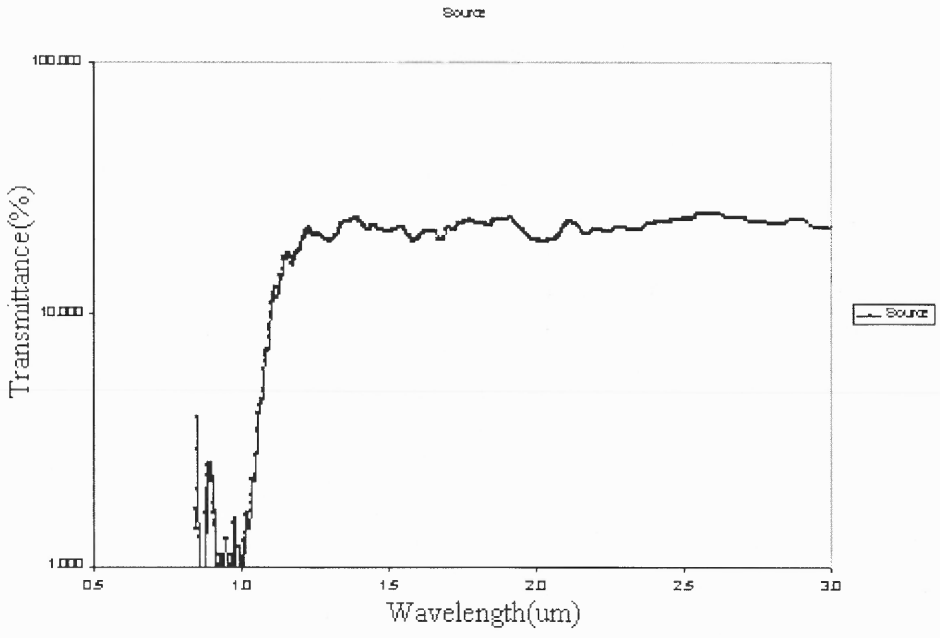

Figure 6.11(a) Transmission spectra for the 3D optical photonic crystal measured experimentally at room temperature (front side)

This is due to the intrinsic bandgap effects in silicon. It is to be noted that the dip in transmittance at 1.5μm (fig. 6.4) is seen very slightly in fig. 6.11(a, b). Our results of the simulation of transmittance of the photonic crystal (figs.6.5, 6.6) are in better agreement with our measured data fig. 6.11(a, b). However, we have been able to see only some

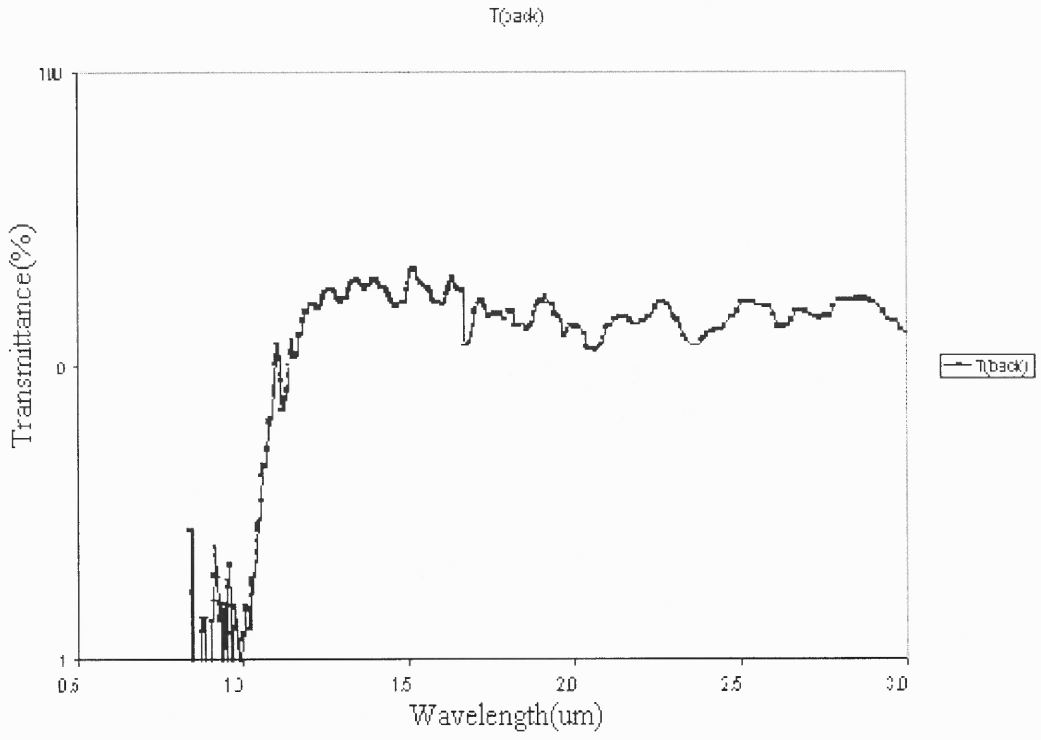

Figure 6.11(b) Transmission spectra for the 3D optical photonic crystal measured experimentally at room temperature (back side)

aspects of the transmittance spectra of the photonic crystal (fig 6.4 and 6.6). We have also been able to demonstrate some limited correspondence to the previously reported characteristics in fig 6.4 in this study.

6.8 Comparisons between Experimental, Simulated and Sandia Data

A comparison chart of all the transmission peaks from experimental, simulated and Sandia (Sandia data in the paper) is compiled below. The table shows the comparisons between the three at room temperature.

Table 1 – Source Temperature

Simulated		Experimental		Sandia	
Wavelength	Peak T	Wavelength	Peak T	Wavelength	Peak T
1.2	62.4	1.16	17.52	1.0	55
1.5	62.4	1.23	21.5	1.1	54
1.9	69.4	1.37	23.62	1.15	50
2.3	62.5	1.91	24.03	1.29	70
		2.11	23.13	2.8	100

Note:- Wavelength is in microns and Peak Transmittance is in %.

As the sample temperature, is increased the peaks differ in intensity as well as position (wavelength). The tables that follow show a comparison between experimental and simulated data at various other temperatures for the same sample with a three layer structure.

Table 2 - 400°C

Simulated		Experimental	
Wavelength	Peak T	Wavelength	Peak T
1.4	65.3	1.45	17.93
1.6	58.7	1.55	17.40
1.9	68.5	1.66	17.69
2.1	64.8	1.74	18.95
2.4	55.6	2.14	18.08
2.7	53.9	2.32	17.35
		2.9	16.26

Table 3 - 560°C

Simulated		Experimental	
Wavelength	Peak T	Wavelength	Peak T
1.4	42.3	1.43	11.61
1.6	50.5	1.58	8.40
1.8	52.2	1.69	8.37
2.0	51.0	1.76	9.73
2.2	45.1	2.18	5.42
2.7	31.9	2.62	5.79

Table 4 - 600°C

Simulated		Experimental	
Wavelength	Peak T	Wavelength	Peak T
1.4	37.1	1.39	17.83
1.6	38.7	1.45	14.48
1.9	42.1	1.57	13.55
		1.76	15.75
		2.15	10.87
		2.33	11.02

As can be seen from the above tables, there is a close match between the points at which the peaks occur, but the significant point of difference is the intensities of the peaks. This may be due to (a) difference in the doping concentration of the silicon wafer, (b) surface roughness of the wafer and (c) possible film thickness variations.

6.9 Reflectance and Emittance of the Photonic Crystal

Even though the reflectance and emittance of the photonic crystal are not under scrutiny, an analysis of their variations is helpful to understand the optical properties.

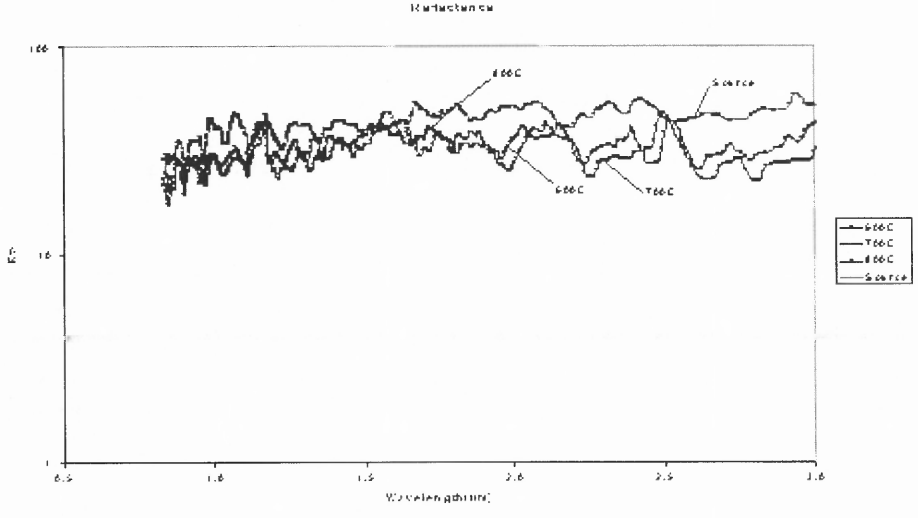

Fig. 6.12 Experimental emittance spectra of the photonic crystal (3L) at different temperatures

In fig 6.12, the measured emittance spectra of a photonic crystal are shown at different temperatures. In general, it can be observed that as the sample temperature is increased, the emittance peaks also increase in intensity for the same wavelength.

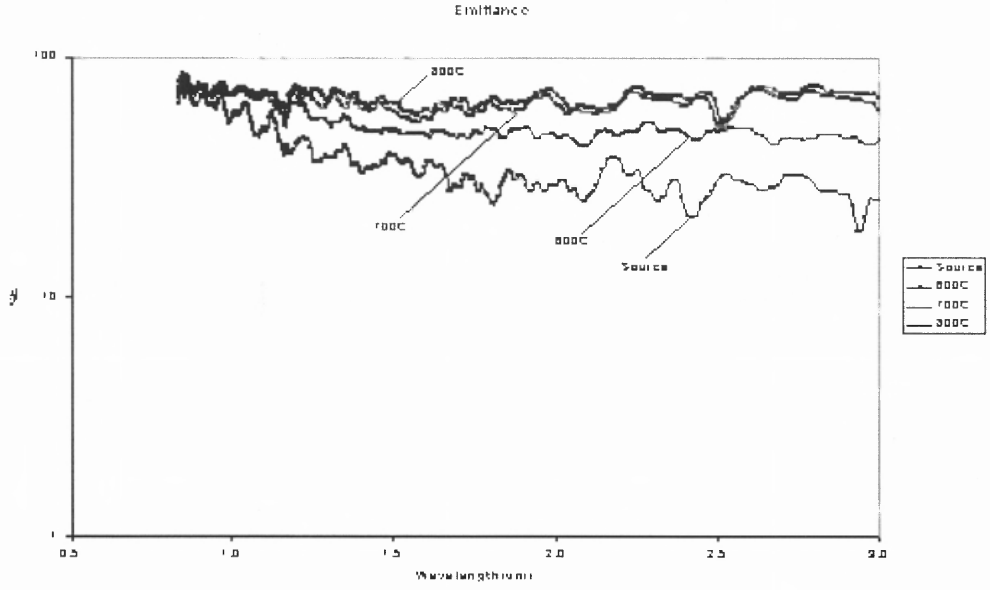

Fig. 6.13 Experimental reflectance spectra of the photonic crystal (3L) at different temperatures

The reflectance spectra for the photonic crystal are shown in fig 6.13. As seen from the fig 6.13, as the temperature is increased, the reflectance decreases for the same wavelength. Also there is an increase in the peak intensity with increase in temperature.

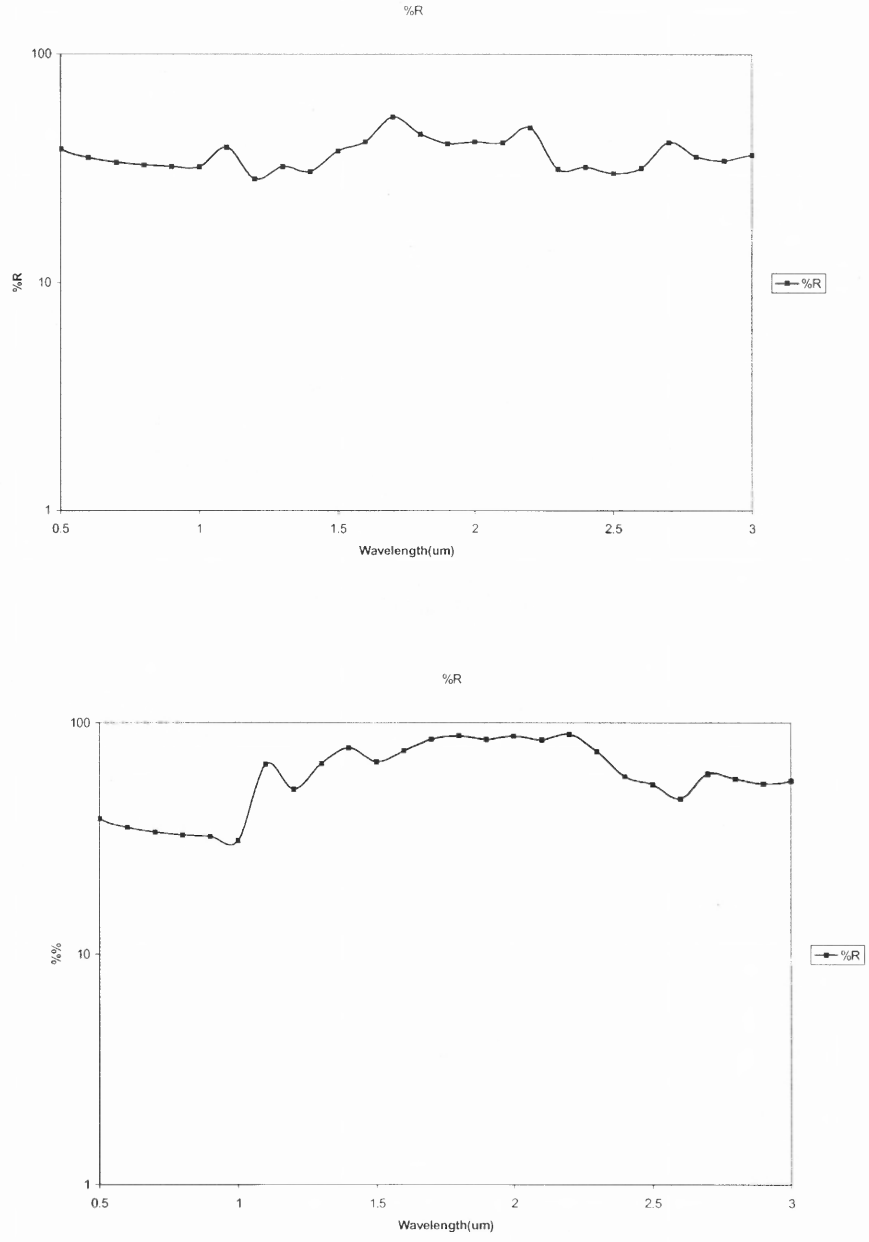

Fig 6.14 Simulated reflectance spectra for a photonic crystal (3L) at different temperatures

In figure 6.14 (a) and (b) are shown the reflectance spectra for a 3 layer photonic crystal. As can be seen from the above figures, at room temperature, the spectra for the photonic crystal cross-section containing SiO_2 is in better agreement with our experimental data.

6.10 The Flip and Angle Case

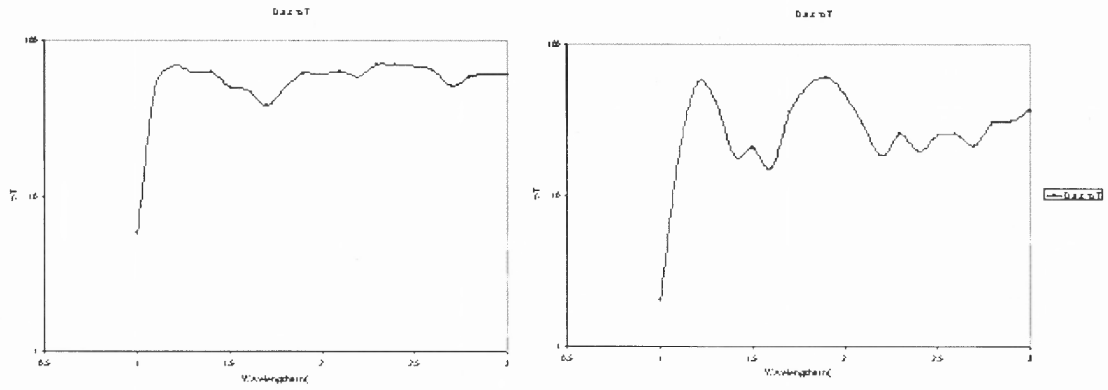

Fig 6.15 Simulated transmittance spectra for a flipped photonic crystal (3L) for (a) Cross-section containing SiO_2 (b) Cross-section containing Poly (both at room temperature)

Now consider the case where the whole stack of layers of the photonic crystal is inverted. In this case, the transmittance spectra of the crystal is as shown in fig 6.15(a) and (b). As can be seen from the above figures, the flip case for the cross-section containing poly shows much more promise than the right side up case. In effect, it means that we can get a better photonic band gap, if the stack of the photonic crystal were to be flipped.

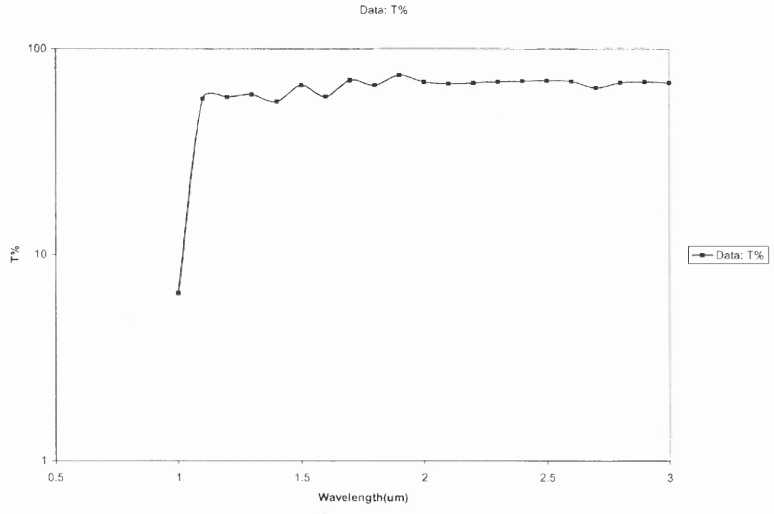

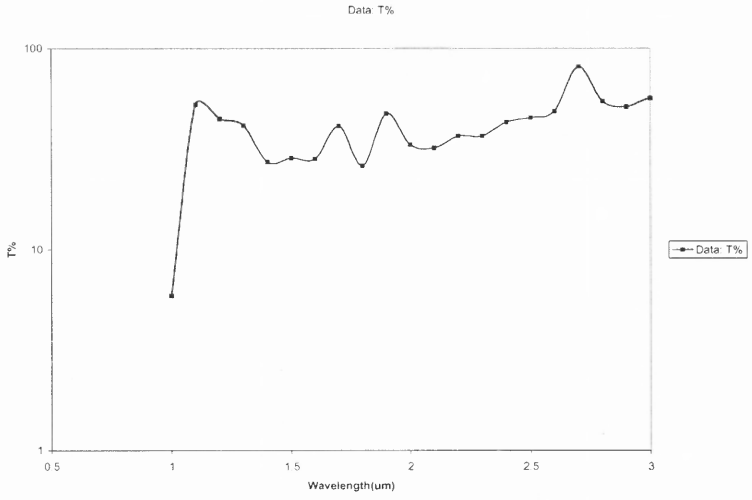

Fig 6.16 Simulated transmittance spectra for a photonic crystal (3L) with 15° angle of incidence for (a) Cross-section containing SiO_2 (b) Cross-section containing Poly (both at room temperature)

Now consider the case where the angle of incidence is 15° to the normal to the plane of incidence. The transmittance spectra in the crystal are as like shown in figure 6.16(a) and (b). As can be seen from the above transmittance spectra, an angle of incidence of 15° seems to cause the cross-section containing SiO_2 to suppress most of the peaks, but in the case of poly we still observe features of a photonic band gap. All this points to the fact that poly silicon is the dominant layer in the photonic crystal that is responsible for the quantum confinement phenomena.

CHAPTER 7

CONCLUSIONS AND RECOMMENDATIONS

7.1 Conclusions

The experimental results presented in this thesis showed that the measurement of high temperature transmissive properties over the wavelength range of 1 to 20 microns and the temperature range of 30 to 800 °C could be performed with relative ease using a novel approach based on the spectral emissometer. It may be noted that in the experiments carried out using the spectral emissometer, measurement was limited to a single point on the sample. In general, the effects of temperature, wavelength, layers, etc on the transmittance of photonic crystals within the available 3mm resolution, leads to the following observations:

- The spectral emissometer fails to show a 100% correspondence with the transmittance characteristics that have been documented in the paper by Flemming and Lin.
- The effect of layers on the structure in general is to reduce transmittance. Thus the lesser the number of layers, the more will it act like a normal crystal with usual transmittance.
- If more defect structures in the crystal can be made, then the transmittance would rapidly go to zero and this property could then be used to trap light and may be used to construct powerful lasers, solar cells and other optoelectronic devices.
- The roughness could also be used to increase light trapping for increased conversion efficiencies in solar cells.

7.2 Recommendations

Much of the work that is being carried out at present seems to be focused on the phenomenon of light trapping. But there is still a long way to go before this energy can be properly harnessed to fabricate devices for potential use in optical communications. It would therefore be a good idea to focus on finding efficient methods to properly control the energy that is being trapped by these photonic crystals. There is a need for (a) fundamental understanding of operation of photonic crystals, (b) ease of fabrication and (c) applications strategies.

APPENDIX A1
TRANSMITTANCE

This appendix gives the values of simulated transmittance of photonic crystals at room temperature (30°C) for a 3-layer structure.

Spectral Range

Increment(μm)	0.1
Minimum Wavelength(μm)	0.4
Maximum Wavelength(μm)	20

Stack Information

Layers	Materials	Thickness (μm)	Temperature (°C)
1	Silicon (-#-)2	300	30
2	Silicon nitride (-#-)5	0.1	30
3	Silicon dioxide (-#-)3	0.22	30
4	Silicon nitride (-#-)5	0.05	30
5	Silicon dioxide (-#-)3	0.22	30
6	Silicon nitride (-#-)5	0.05	30
7	Silicon dioxide (-#-)3	0.22	30
8	Silicon nitride (-#-)5	0.05	30

Wave Length(μm)	T(%) - 3L(SiO_2)	T(%) - 4L(SiO_2)	T(%) - 3L(Poly)	T(%) - 4L(Poly)
0.4	0	0	0	0
0.5	0	0	0	0
0.6	0	0	0	0
0.7	0	0	0	0
0.8	0	0	0	0
0.9	0	0	0	0
1	4.8	5.1	1.7	2.7
1.1	56	58.1	39.6	35.6
1.2	62.4	49.6	58	53.2
1.3	61.5	62	59.6	56.3

1.4	54.9	58.3	44.6	64.1
1.5	62.4	70.9	68.7	65.7
1.6	49	58.8	62.1	59.6
1.7	58.9	47.8	35.1	29.6
1.8	65	55.3	28.7	20.5
1.9	69.4	59.1	38.9	29.7
2	68.1	58.5	31.1	27.8
2.1	64.2	58.6	35.7	41.8
2.2	55.7	52.6	49.1	69.2
2.3	62.5	68.9	52.6	57.4
2.4	59.4	67.5	58.7	49.6
2.5	58.6	69.2	61.3	48.8
2.6	52.6	65.6	55	45.6
2.7	34	51.7	33.6	60.1
2.8	49.4	60.8	44.2	53.4
2.9	55.6	63.3	47.8	48.9
3	57.4	62	46.4	54.5
3.1	57.1	61.8	41.2	57
3.2	55.1	56.8	48.4	57.6
3.3	57.9	55	46.3	58.7
3.4	57.6	54.9	48.7	56.5
3.5	57.3	53.8	51.8	53.9
3.6	57.6	53	54.7	50.9
3.7	56.9	49.7	58.7	48.2
3.8	85.4	88.4	34.1	67.3
3.9	77.6	75.1	38.8	63
4	58.6	49.8	60.9	47.5
4.1	62.2	55.2	61.5	45.6
4.2	64.2	55.3	56.9	53.6
4.3	63.9	55.9	59.5	50.4
4.4	63.3	54.2	58.9	52.7
4.5	64.9	57	58.7	51.3
4.6	64.4	56.5	59.2	54.2
4.7	66.6	60.8	55.8	55.8
4.8	65.7	58.9	55	58.7
4.9	66.3	59.7	57.5	57.8
5	66.4	60.1	56	56.1
5.1	66.2	60.3	55	58.7
5.2	67	62.7	53.6	58.1
5.3	67.8	63	56.5	56
5.4	64.9	60.1	45.1	63
5.5	66.2	61	47.1	59.5
5.6	66.9	64.6	54	58.5
5.7	67.2	65.3	54	56.1
5.8	67.5	66.1	53.9	59.2
5.9	67.6	66.4	53.6	58.3
6	65.9	65.6	53.2	56.8
6.1	65.9	65.5	51.9	57.9
6.2	64.7	64.3	49	57.8

6.3	64	65	51.8	53.9
6.4	64.2	65.4	53.2	55.1
6.5	63.3	64.7	53.1	53.7
6.6	64.2	65.4	48	56.2
6.7	63.1	64.8	49	55.1
6.8	63.2	64.6	51.3	54.3
6.9	59.5	61.4	50.7	50.9
7	61.1	63.1	52.9	54.2
7.1	62.2	63.9	52.7	55.6
7.2	61.5	63.1	51.6	55.7
7.3	59.4	61	52.8	53.7
7.4	58.6	59.9	52	52.4
7.5	57.7	58.7	51.7	52.7
7.6	54.7	55.4	53	50.1
7.7	57.2	57.4	53.4	53.6
7.8	51.1	50.5	50.9	49.2
7.9	50.6	49	55.2	53.5
8	50.9	47.9	51.7	54.9
8.1	46.3	42.1	50.2	50.8
8.2	41.8	36.9	50.8	50.1
8.3	39.8	34.4	51.4	50.2
8.4	38.2	32.4	51.9	50.6
8.5	37	30.7	52.2	51.1
8.6	34.6	28	52.7	50.8
8.7	33.5	26.5	51.1	50.7
8.8	30.9	23.2	53.5	51.9
8.9	23	15.4	53.6	49
9	16	8.9	50.9	52
9.1	8.7	4.1	55.7	50.9
9.2	7.3	3.4	51.5	53.4
9.3	7.7	3.8	54	47.7
9.4	10.5	5.8	57.3	55.4
9.5	12.3	7.5	50.8	51.7
9.6	15.3	10.1	52.1	48.4
9.7	20.7	14.9	57.2	50.4
9.8	26.7	21	58.3	54.5
9.9	31.6	27	55.3	55.9
10	37.3	33.5	53.6	54.5
10.1	41.3	38.1	52.9	52.8
10.2	46	43.6	52.8	52.1
10.3	50.3	48.9	53	52
10.4	53.2	52.5	53.5	51.7
10.5	56.1	56.3	53.4	51
10.6	58.2	59.3	53	51.2
10.7	59.1	61.9	53.7	51.8
10.8	60.8	64.8	54.3	51.7
10.9	61.9	65.2	53.2	48.3
11	61	63.9	49.4	50.2
11.1	56.5	61.8	54.3	52.7

11.2	60.3	64	53.8	48.2
11.3	59.7	62.6	48.6	50.7
11.4	54.6	59.6	56.1	53.4
11.5	58.6	60.3	48.6	46
11.6	50.2	53.4	56.5	55.6
11.7	56.2	56.7	50.5	45.9
11.8	48.1	50.1	57.5	57.1
11.9	54.2	53.6	49.4	46.4
12	45.4	46.3	59	56.7
12.1	49.5	48.4	47.7	49.2
12.2	45.8	44.8	56.9	49.6
12.3	43.3	43.2	53.8	57.1
12.4	48.7	46.6	48.4	46.6
12.5	45.1	44.3	59	52.1
12.6	43.5	43.7	54.4	57.9
12.7	48.4	47.1	48.1	48.1
12.8	49.8	48.6	53.1	47.7
12.9	46.1	47	59.4	55.6
13	46.1	47.3	52.6	56.7
13.1	49.6	50	48.7	49.4
13.2	53.5	53	49.6	47.4
13.3	51.9	52.5	53.7	48.8
13.4	48.5	50.1	57.6	52.6
13.5	46.9	48.6	55.4	55.9
13.6	47.1	48.6	51.8	54.8
13.7	47.9	49.3	50.1	51.8
13.8	49.7	50.8	50.2	50.6
13.9	51.3	52.1	50.9	50.6
14	52.6	53.2	51.7	51
14.1	53.5	53.9	52.6	51.7
14.2	53.9	54.3	53.4	52.4
14.3	54	54.4	54.1	53.1
14.4	53.5	53.9	54.3	53.4
14.5	52.9	53.4	54.4	53.7
14.6	52.2	52.8	54.6	53.9
14.7	51.7	52.3	54.7	54.2
14.8	51.4	52	55.1	54.6
14.9	51.3	51.9	55.4	54.9
15	51.4	51.9	55.6	54.8
15.1	51.6	52	55.4	54.1
15.2	51.7	52	54.5	52.8
15.3	51.5	51.7	52.7	52.8
15.4	50.4	50.6	52.7	54.5
15.5	48.1	48.6	54.9	55.9
15.6	47.6	48.3	56.6	56.7
15.7	48.9	49.1	55.7	54.9
15.8	48.7	48.6	52.7	50.2
15.9	46.9	46.7	46.8	44.8
16	42.7	42.6	43.5	46.3

16.1	37.7	38.3	46	47.2
16.2	39.4	39.6	46.8	46.4
16.3	41.6	41.4	44.8	42.2
16.4	40.5	40.3	38.8	38.6
16.5	35.1	35.3	40.2	42.9
16.6	38.4	38.7	48.5	48.7
16.7	46.3	45.8	50.7	47.2
16.8	46.8	46.1	42.4	42.8
16.9	39.4	39.8	50.7	54.5
17	46	45.7	57.4	56.5
17.1	51.1	50.1	50.5	44.7
17.2	43.9	43.4	45.1	51.5
17.3	41.8	41.9	58.2	59
17.4	51.3	50.2	54.3	48.3
17.5	45.2	44.4	41.9	47.6
17.6	39.7	39.8	57.9	59.4
17.7	51.6	50.3	54.6	48.2
17.8	44	43.2	41.9	48.5
17.9	41.3	41	59.9	60.7
18	52.6	51.1	51.2	44
18.1	39.1	38.8	46.3	54.2
18.2	47.1	46	61.7	59.9
18.3	51.4	49.8	42.1	40.1
18.4	35.8	35.9	56.9	61.5
18.5	53.5	51.8	57.6	50.4
18.6	41.4	40.8	41.8	49.9
18.7	46.2	45.1	63.6	62.3
18.8	52.1	50.5	40.7	39.3
18.9	36.2	36.1	60.1	64
19	55.9	54.1	52.4	44.1
19.1	35.3	35.1	49.2	58.1
19.2	54	52.2	62	55.4
19.3	41.4	40.6	40	47.7
19.4	47.9	46.1	65.8	63.1
19.5	48.4	46.9	37.6	40.4
19.6	40.9	39.4	66.2	66.6
19.7	52.7	50.6	39.3	38
19.8	35.4	33.8	64.8	67.6
19.9	54.6	52	42.2	38.1
20	32.5	30.8	63	67.7

APPENDIX A2
RAW DATA

This appendix gives the raw data obtained from experiments performed on the sample at Advanced Fuel Research (AFR)

Source Temp, **Front**		Source Temp, **Back**	
Trans(%)	λ(μm)	Trans(%)	λ(μm)
0.460	19.642	0.398	19.642
0.460	19.064	0.316	19.064
0.460	18.520	0.301	18.520
0.431	18.005	0.269	18.005
0.388	17.518	0.234	17.518
0.332	17.057	0.197	17.057
0.236	16.620	0.152	16.620
0.236	16.205	0.137	16.205
0.236	15.809	0.134	15.809
0.205	15.433	0.121	15.433
0.203	15.074	0.118	15.074
0.174	14.731	0.099	14.731
0.146	14.404	0.086	14.404
0.118	14.091	0.068	14.091
0.089	13.791	0.054	13.791
0.074	13.504	0.044	13.504
0.065	13.228	0.040	13.228
0.060	12.964	0.035	12.964
0.054	12.709	0.033	12.709
0.049	12.465	0.030	12.465
0.044	12.230	0.029	12.230
0.041	12.003	0.027	12.003
0.038	11.785	0.024	11.785
0.035	11.575	0.023	11.575
0.032	11.372	0.022	11.372
0.032	11.176	0.021	11.176
0.032	10.986	0.021	10.986
0.035	10.803	0.021	10.803
0.037	10.626	0.026	10.626
0.041	10.455	0.028	10.455
0.046	10.289	0.033	10.289
0.055	10.128	0.040	10.128
0.068	9.972	0.052	9.972
0.087	9.821	0.071	9.821
0.111	9.674	0.093	9.674
0.142	9.532	0.120	9.532
0.173	9.394	0.120	9.394
0.173	9.260	0.120	9.260
0.174	9.129	0.114	9.129

APPENDIX A2
(CONTINUED)

0.174	8.879	0.108	8.879
0.172	8.759	0.104	8.759
0.169	8.642	0.097	8.642
0.169	8.529	0.084	8.529
0.164	8.418	0.070	8.418
0.158	8.310	0.066	8.310
0.158	8.205	0.066	8.205
0.139	8.102	0.066	8.102
0.120	8.002	0.068	8.002
0.120	7.905	0.070	7.905
0.120	7.809	0.071	7.809
0.133	7.716	0.073	7.716
0.137	7.626	0.079	7.626
0.139	7.537	0.084	7.537
0.139	7.450	0.074	7.450
0.138	7.366	0.074	7.366
0.138	7.283	0.074	7.283
0.125	7.202	0.074	7.202
0.105	7.123	0.074	7.123
0.105	7.045	0.080	7.045
0.105	6.970	0.085	6.970
0.109	6.896	0.093	6.896
0.135	6.823	0.105	6.823
0.145	6.752	0.108	6.752
0.145	6.682	0.114	6.682
0.148	6.614	0.135	6.614
0.153	6.547	0.144	6.547
0.159	6.482	0.144	6.482
0.163	6.418	0.144	6.418
0.163	6.355	0.122	6.355
0.167	6.293	0.100	6.293
0.167	6.233	0.087	6.233
0.167	6.173	0.087	6.173
0.172	6.115	0.087	6.115
0.184	6.058	0.103	6.058
0.198	6.002	0.126	6.002
0.207	5.947	0.155	5.947
0.221	5.893	0.193	5.893
0.221	5.839	0.193	5.839
0.221	5.787	0.193	5.787
0.212	5.736	0.155	5.736
0.212	5.686	0.133	5.686
0.212	5.636	0.133	5.636
0.213	5.588	0.133	5.588
0.213	5.540	0.138	5.540
0.221	5.493	0.160	5.493
0.221	5.447	0.170	5.447
0.227	5.402	0.170	5.402

APPENDIX A2
(CONTINUED)

0.232	5.357	0.170	5.357
0.231	5.313	0.167	5.313
0.231	5.270	0.163	5.270
0.231	5.227	0.154	5.227
0.202	5.185	0.141	5.185
0.192	5.144	0.141	5.144
0.185	5.104	0.135	5.104
0.185	5.064	0.135	5.064
0.185	5.025	0.133	5.025
0.192	4.986	0.133	4.986
0.197	4.948	0.133	4.948
0.200	4.910	0.141	4.910
0.201	4.874	0.142	4.874
0.209	4.837	0.146	4.837
0.228	4.801	0.146	4.801
0.228	4.766	0.146	4.766
0.228	4.731	0.125	4.731
0.216	4.697	0.113	4.697
0.216	4.663	0.112	4.663
0.214	4.630	0.108	4.630
0.213	4.597	0.108	4.597
0.213	4.565	0.097	4.565
0.214	4.533	0.097	4.533
0.214	4.501	0.097	4.501
0.212	4.470	0.106	4.470
0.208	4.440	0.129	4.440
0.207	4.409	0.129	4.409
0.207	4.380	0.129	4.380
0.207	4.350	0.122	4.350
0.207	4.321	0.122	4.321
0.212	4.293	0.122	4.293
0.232	4.264	0.125	4.264
0.232	4.236	0.140	4.236
0.232	4.209	0.144	4.209
0.232	4.182	0.144	4.182
0.232	4.155	0.144	4.155
0.232	4.129	0.139	4.129
0.236	4.102	0.138	4.102
0.240	4.077	0.133	4.077
0.251	4.051	0.133	4.051
0.251	4.026	0.133	4.026
0.251	4.001	0.135	4.001
0.244	3.977	0.135	3.977
0.235	3.952	0.135	3.952
0.227	3.928	0.121	3.928
0.217	3.905	0.116	3.905
0.207	3.881	0.113	3.881
0.207	3.858	0.113	3.858

APPENDIX A2
(CONTINUED)

0.207	3.835	0.116	3.835
0.210	3.813	0.114	3.813
0.210	3.791	0.114	3.791
0.210	3.769	0.114	3.769
0.209	3.747	0.094	3.747
0.205	3.725	0.094	3.725
0.196	3.704	0.089	3.704
0.195	3.683	0.088	3.683
0.195	3.662	0.089	3.662
0.195	3.641	0.089	3.641
0.198	3.621	0.089	3.621
0.199	3.601	0.091	3.601
0.200	3.581	0.094	3.581
0.202	3.561	0.116	3.561
0.209	3.542	0.126	3.542
0.216	3.523	0.128	3.523
0.220	3.504	0.128	3.504
0.225	3.485	0.127	3.485
0.237	3.466	0.126	3.466
0.249	3.448	0.123	3.448
0.253	3.430	0.123	3.430
0.259	3.411	0.123	3.411
0.268	3.394	0.138	3.394
0.271	3.376	0.138	3.376
0.273	3.358	0.138	3.358
0.273	3.341	0.134	3.341
0.273	3.324	0.123	3.324
0.267	3.307	0.122	3.307
0.259	3.290	0.119	3.290
0.253	3.274	0.118	3.274
0.250	3.257	0.118	3.257
0.250	3.241	0.117	3.241
0.248	3.225	0.114	3.225
0.248	3.209	0.113	3.209
0.248	3.193	0.113	3.193
0.244	3.177	0.110	3.177
0.242	3.162	0.103	3.162
0.237	3.147	0.103	3.147
0.235	3.131	0.103	3.131
0.235	3.116	0.105	3.116
0.235	3.101	0.106	3.101
0.236	3.087	0.109	3.087
0.236	3.072	0.109	3.072
0.236	3.057	0.113	3.057
0.236	3.043	0.123	3.043
0.232	3.029	0.128	3.029
0.227	3.015	0.130	3.015
0.223	3.001	0.131	3.001

APPENDIX A2
(CONTINUED)

0.221	2.987	0.133	2.987
0.221	2.973	0.143	2.973
0.221	2.960	0.143	2.960
0.222	2.946	0.145	2.946
0.226	2.933	0.153	2.933
0.232	2.920	0.161	2.920
0.236	2.907	0.167	2.907
0.238	2.894	0.167	2.894
0.238	2.881	0.169	2.881
0.238	2.868	0.169	2.868
0.233	2.855	0.169	2.855
0.228	2.843	0.169	2.843
0.228	2.830	0.169	2.830
0.228	2.818	0.169	2.818
0.228	2.806	0.168	2.806
0.228	2.794	0.168	2.794
0.231	2.782	0.158	2.782
0.234	2.770	0.148	2.770
0.234	2.758	0.148	2.758
0.234	2.747	0.147	2.747
0.234	2.735	0.147	2.735
0.234	2.723	0.148	2.723
0.239	2.712	0.150	2.712
0.243	2.701	0.153	2.701
0.243	2.690	0.154	2.690
0.243	2.678	0.154	2.678
0.242	2.667	0.154	2.667
0.242	2.656	0.144	2.656
0.242	2.646	0.137	2.646
0.247	2.635	0.136	2.635
0.251	2.624	0.136	2.624
0.252	2.614	0.136	2.614
0.252	2.603	0.149	2.603
0.252	2.593	0.159	2.593
0.252	2.582	0.160	2.582
0.250	2.572	0.160	2.572
0.249	2.562	0.161	2.562
0.248	2.552	0.161	2.552
0.244	2.542	0.166	2.542
0.240	2.532	0.166	2.532
0.240	2.522	0.166	2.522
0.239	2.512	0.166	2.512
0.240	2.503	0.166	2.503
0.239	2.493	0.154	2.493
0.238	2.483	0.148	2.483
0.238	2.474	0.147	2.474
0.235	2.465	0.141	2.465
0.234	2.455	0.135	2.455

APPENDIX A2
(CONTINUED)

0.232	2.446	0.133	2.446
0.232	2.437	0.133	2.437
0.232	2.428	0.132	2.428
0.232	2.419	0.131	2.419
0.232	2.410	0.131	2.410
0.230	2.401	0.127	2.401
0.229	2.392	0.125	2.392
0.228	2.383	0.123	2.383
0.226	2.374	0.118	2.374
0.221	2.366	0.118	2.366
0.217	2.357	0.118	2.357
0.215	2.348	0.120	2.348
0.215	2.340	0.123	2.340
0.215	2.332	0.127	2.332
0.215	2.323	0.136	2.323
0.218	2.315	0.144	2.315
0.221	2.307	0.146	2.307
0.222	2.299	0.148	2.299
0.222	2.290	0.156	2.290
0.222	2.282	0.162	2.282
0.219	2.274	0.165	2.274
0.216	2.266	0.165	2.266
0.212	2.258	0.165	2.258
0.212	2.251	0.158	2.251
0.212	2.243	0.154	2.243
0.213	2.235	0.150	2.235
0.216	2.227	0.147	2.227
0.218	2.220	0.147	2.220
0.218	2.212	0.143	2.212
0.218	2.205	0.141	2.205
0.217	2.197	0.139	2.197
0.212	2.190	0.139	2.190
0.210	2.182	0.139	2.182
0.210	2.175	0.140	2.175
0.210	2.168	0.144	2.168
0.213	2.161	0.148	2.161
0.219	2.153	0.148	2.153
0.226	2.146	0.148	2.146
0.228	2.139	0.148	2.139
0.229	2.132	0.145	2.132
0.231	2.125	0.145	2.125
0.231	2.118	0.145	2.118
0.231	2.111	0.138	2.111
0.228	2.104	0.136	2.104
0.224	2.098	0.135	2.098
0.218	2.091	0.125	2.091
0.210	2.084	0.118	2.084
0.204	2.078	0.116	2.078

APPENDIX A2
(CONTINUED)

0.200	2.071	0.114	2.071
0.197	2.064	0.113	2.064
0.197	2.058	0.114	2.058
0.197	2.051	0.114	2.051
0.197	2.045	0.114	2.045
0.193	2.038	0.118	2.038
0.193	2.032	0.129	2.032
0.193	2.026	0.131	2.026
0.195	2.019	0.134	2.019
0.196	2.013	0.135	2.013
0.196	2.007	0.137	2.007
0.196	2.001	0.135	2.001
0.196	1.994	0.139	1.994
0.196	1.988	0.139	1.988
0.200	1.982	0.133	1.982
0.205	1.976	0.128	1.976
0.210	1.970	0.128	1.970
0.213	1.964	0.128	1.964
0.216	1.958	0.143	1.958
0.217	1.952	0.148	1.952
0.221	1.946	0.150	1.946
0.223	1.941	0.151	1.941
0.228	1.935	0.162	1.935
0.235	1.929	0.163	1.929
0.240	1.923	0.163	1.923
0.240	1.918	0.173	1.918
0.240	1.912	0.172	1.912
0.239	1.906	0.166	1.906
0.238	1.901	0.168	1.901
0.237	1.895	0.168	1.895
0.236	1.890	0.166	1.890
0.236	1.884	0.160	1.884
0.236	1.879	0.151	1.879
0.235	1.873	0.139	1.873
0.235	1.868	0.136	1.868
0.235	1.863	0.133	1.863
0.234	1.857	0.133	1.857
0.225	1.852	0.133	1.852
0.225	1.847	0.139	1.847
0.225	1.841	0.139	1.841
0.226	1.836	0.139	1.836
0.228	1.831	0.137	1.831
0.228	1.826	0.137	1.826
0.231	1.821	0.137	1.821
0.231	1.816	0.153	1.816
0.231	1.811	0.154	1.811
0.231	1.806	0.154	1.806
0.231	1.801	0.154	1.801

APPENDIX A2
(CONTINUED)

0.232	1.796	0.145	1.796
0.234	1.791	0.145	1.791
0.234	1.786	0.145	1.786
0.234	1.781	0.151	1.781
0.237	1.776	0.151	1.776
0.234	1.771	0.151	1.771
0.232	1.766	0.151	1.766
0.232	1.761	0.151	1.761
0.231	1.757	0.150	1.757
0.229	1.752	0.150	1.752
0.228	1.747	0.148	1.747
0.228	1.742	0.148	1.742
0.227	1.738	0.148	1.738
0.221	1.733	0.157	1.733
0.218	1.728	0.160	1.728
0.217	1.724	0.167	1.724
0.217	1.719	0.167	1.719
0.218	1.715	0.164	1.715
0.221	1.710	0.164	1.710
0.221	1.706	0.157	1.706
0.221	1.701	0.153	1.701
0.217	1.697	0.136	1.697
0.203	1.692	0.128	1.692
0.198	1.688	0.122	1.688
0.197	1.684	0.120	1.684
0.197	1.679	0.118	1.679
0.197	1.675	0.118	1.675
0.198	1.671	0.118	1.671
0.211	1.666	0.180	1.666
0.211	1.662	0.180	1.662
0.213	1.658	0.181	1.658
0.214	1.654	0.181	1.654
0.214	1.649	0.184	1.649
0.214	1.645	0.189	1.645
0.212	1.641	0.197	1.641
0.212	1.637	0.200	1.637
0.212	1.633	0.200	1.633
0.212	1.629	0.200	1.629
0.211	1.625	0.193	1.625
0.210	1.620	0.184	1.620
0.210	1.616	0.177	1.616
0.206	1.612	0.167	1.612
0.202	1.608	0.162	1.608
0.200	1.604	0.162	1.604
0.198	1.600	0.162	1.600
0.196	1.597	0.164	1.597
0.196	1.593	0.165	1.593
0.196	1.589	0.166	1.589

APPENDIX A2
(CONTINUED)

0.196	1.585	0.166	1.585
0.196	1.581	0.166	1.581
0.202	1.577	0.167	1.577
0.206	1.573	0.169	1.573
0.206	1.569	0.173	1.569
0.207	1.566	0.180	1.566
0.213	1.562	0.184	1.562
0.217	1.558	0.185	1.558
0.218	1.554	0.186	1.554
0.219	1.551	0.187	1.551
0.220	1.547	0.188	1.547
0.220	1.543	0.190	1.543
0.220	1.540	0.192	1.540
0.220	1.536	0.195	1.536
0.220	1.532	0.197	1.532
0.218	1.529	0.199	1.529
0.217	1.525	0.203	1.525
0.216	1.522	0.210	1.522
0.215	1.518	0.214	1.518
0.214	1.514	0.214	1.514
0.213	1.511	0.214	1.511
0.212	1.507	0.212	1.507
0.212	1.504	0.203	1.504
0.212	1.500	0.192	1.500
0.212	1.497	0.182	1.497
0.214	1.494	0.167	1.494
0.214	1.490	0.167	1.490
0.214	1.487	0.167	1.487
0.215	1.483	0.165	1.483
0.215	1.480	0.165	1.480
0.216	1.476	0.164	1.476
0.216	1.473	0.164	1.473
0.217	1.470	0.162	1.470
0.218	1.466	0.161	1.466
0.222	1.463	0.160	1.463
0.224	1.460	0.160	1.460
0.225	1.457	0.160	1.457
0.225	1.453	0.164	1.453
0.224	1.450	0.167	1.450
0.224	1.447	0.169	1.447
0.223	1.444	0.171	1.444
0.221	1.440	0.175	1.440
0.216	1.437	0.181	1.437
0.216	1.434	0.184	1.434
0.216	1.431	0.187	1.431
0.216	1.428	0.187	1.428
0.218	1.425	0.187	1.425
0.221	1.421	0.186	1.421

APPENDIX A2
(CONTINUED)

0.223	1.418	0.186	1.418
0.224	1.415	0.186	1.415
0.229	1.412	0.189	1.412
0.231	1.409	0.192	1.409
0.233	1.406	0.194	1.406
0.235	1.403	0.197	1.403
0.237	1.400	0.199	1.400
0.240	1.397	0.199	1.397
0.240	1.394	0.199	1.394
0.240	1.391	0.194	1.391
0.240	1.388	0.190	1.388
0.240	1.385	0.190	1.385
0.237	1.382	0.189	1.382
0.236	1.379	0.189	1.379
0.236	1.376	0.189	1.376
0.236	1.373	0.186	1.373
0.235	1.370	0.183	1.370
0.234	1.367	0.183	1.367
0.233	1.365	0.183	1.365
0.233	1.362	0.188	1.362
0.232	1.359	0.190	1.359
0.232	1.356	0.192	1.356
0.232	1.353	0.192	1.353
0.232	1.350	0.196	1.350
0.230	1.348	0.198	1.348
0.229	1.345	0.198	1.345
0.229	1.342	0.198	1.342
0.226	1.339	0.196	1.339
0.220	1.336	0.196	1.336
0.218	1.334	0.195	1.334
0.210	1.331	0.195	1.331
0.206	1.328	0.193	1.328
0.203	1.326	0.189	1.326
0.203	1.323	0.182	1.323
0.203	1.320	0.176	1.320
0.200	1.317	0.172	1.317
0.198	1.315	0.172	1.315
0.198	1.312	0.172	1.312
0.196	1.309	0.171	1.309
0.197	1.307	0.171	1.307
0.195	1.304	0.171	1.304
0.195	1.302	0.169	1.302
0.196	1.299	0.168	1.299
0.196	1.296	0.168	1.296
0.196	1.294	0.168	1.294
0.196	1.291	0.168	1.291
0.196	1.289	0.170	1.289
0.198	1.286	0.170	1.286

APPENDIX A2
(CONTINUED)

0.198	1.284	0.172	1.284
0.200	1.281	0.177	1.281
0.200	1.278	0.178	1.278
0.201	1.276	0.179	1.276
0.203	1.273	0.182	1.273
0.204	1.271	0.182	1.271
0.206	1.268	0.182	1.268
0.207	1.266	0.182	1.266
0.209	1.264	0.182	1.264
0.210	1.261	0.182	1.261
0.210	1.259	0.182	1.259
0.210	1.256	0.182	1.256
0.209	1.254	0.180	1.254
0.203	1.251	0.180	1.251
0.203	1.249	0.178	1.249
0.203	1.247	0.178	1.247
0.203	1.244	0.177	1.244
0.205	1.242	0.172	1.242
0.207	1.239	0.166	1.239
0.212	1.237	0.163	1.237
0.218	1.235	0.162	1.235
0.220	1.232	0.160	1.232
0.220	1.230	0.158	1.230
0.220	1.228	0.158	1.228
0.215	1.225	0.158	1.225
0.211	1.223	0.163	1.223
0.207	1.221	0.163	1.221
0.211	1.218	0.164	1.218
0.204	1.216	0.163	1.216
0.202	1.214	0.162	1.214
0.202	1.212	0.162	1.212
0.199	1.209	0.164	1.209
0.197	1.207	0.162	1.207
0.191	1.205	0.162	1.205
0.186	1.203	0.162	1.203
0.181	1.200	0.160	1.200
0.180	1.198	0.153	1.198
0.176	1.196	0.153	1.196
0.177	1.194	0.153	1.194
0.177	1.192	0.153	1.192
0.176	1.189	0.153	1.189
0.174	1.187	0.153	1.187
0.173	1.185	0.151	1.185
0.168	1.183	0.145	1.183
0.162	1.181	0.143	1.181
0.160	1.179	0.142	1.179
0.157	1.176	0.129	1.176
0.157	1.174	0.129	1.174

APPENDIX A2
(CONTINUED)

0.158	1.172	0.129	1.172
0.158	1.170	0.127	1.170
0.169	1.168	0.110	1.168
0.171	1.166	0.110	1.166
0.175	1.164	0.108	1.164
0.175	1.162	0.108	1.162
0.175	1.160	0.108	1.160
0.168	1.157	0.109	1.157
0.165	1.155	0.109	1.155
0.165	1.153	0.109	1.153
0.168	1.151	0.118	1.151
0.165	1.149	0.123	1.149
0.166	1.147	0.123	1.147
0.166	1.145	0.118	1.145
0.165	1.143	0.113	1.143
0.151	1.141	0.111	1.141
0.138	1.139	0.102	1.139
0.138	1.137	0.094	1.137
0.138	1.135	0.085	1.135
0.142	1.133	0.083	1.133
0.142	1.131	0.078	1.131
0.142	1.129	0.078	1.129
0.142	1.127	0.078	1.127
0.117	1.125	0.078	1.125
0.117	1.123	0.071	1.123
0.128	1.121	0.078	1.121
0.128	1.119	0.078	1.119
0.128	1.118	0.071	1.118
0.128	1.116	0.089	1.116
0.127	1.114	0.094	1.114
0.122	1.112	0.107	1.112
0.119	1.110	0.109	1.110
0.115	1.108	0.109	1.108
0.110	1.106	0.119	1.106
0.110	1.104	0.109	1.104
0.101	1.102	0.106	1.102
0.098	1.100	0.102	1.100
0.090	1.099	0.084	1.099
0.087	1.097	0.083	1.097
0.081	1.095	0.080	1.095
0.073	1.093	0.076	1.093
0.073	1.091	0.071	1.091
0.072	1.089	0.067	1.089
0.071	1.088	0.063	1.088
0.071	1.086	0.063	1.086
0.068	1.084	0.067	1.084
0.065	1.082	0.067	1.082
0.065	1.080	0.066	1.080

APPENDIX A2
(CONTINUED)

0.060	1.079	0.066	1.079
0.051	1.077	0.065	1.077
0.050	1.075	0.064	1.075
0.046	1.073	0.052	1.073
0.046	1.071	0.046	1.071
0.045	1.070	0.046	1.070
0.045	1.068	0.045	1.068
0.045	1.066	0.045	1.066
0.043	1.064	0.045	1.064
0.043	1.063	0.046	1.063
0.043	1.061	0.045	1.061
0.041	1.059	0.044	1.059
0.041	1.057	0.043	1.057
0.035	1.056	0.035	1.056
0.034	1.054	0.030	1.054
0.028	1.052	0.030	1.052
0.028	1.051	0.030	1.051
0.023	1.049	0.029	1.049
0.022	1.047	0.029	1.047
0.022	1.045	0.028	1.045
0.022	1.044	0.026	1.044
0.022	1.042	0.023	1.042
0.022	1.040	0.022	1.040
0.022	1.039	0.022	1.039
0.022	1.037	0.022	1.037
0.019	1.035	0.020	1.035
0.018	1.034	0.019	1.034
0.016	1.032	0.017	1.032
0.014	1.030	0.017	1.030
0.014	1.029	0.017	1.029
0.014	1.027	0.019	1.027
0.014	1.026	0.019	1.026
0.015	1.024	0.019	1.024
0.016	1.022	0.018	1.022
0.016	1.021	0.017	1.021
0.016	1.019	0.013	1.019
0.016	1.018	0.013	1.018
0.013	1.016	0.013	1.016
0.013	1.014	0.015	1.014
0.013	1.013	0.015	1.013
0.011	1.011	0.015	1.011
0.013	1.010	0.015	1.010
0.011	1.008	0.015	1.008
0.009	1.006	0.015	1.006
0.010	1.005	0.012	1.005
0.010	1.003	0.012	1.003
0.010	1.002	0.012	1.002
0.010	1.000	0.012	1.000

APPENDIX A2
(CONTINUED)

0.010	0.999	0.012	0.999
0.012	0.997	0.012	0.997
0.012	0.996	0.009	0.996
0.010	0.994	0.007	0.994
0.010	0.993	0.007	0.993
0.010	0.991	0.009	0.991
0.006	0.990	0.011	0.990
0.006	0.988	0.011	0.988
0.006	0.987	0.011	0.987
0.006	0.985	0.011	0.985
0.010	0.984	0.011	0.984
0.013	0.982	0.012	0.982
0.015	0.981	0.013	0.981
0.015	0.979	0.014	0.979
0.015	0.978	0.015	0.978
0.015	0.976	0.015	0.976
0.011	0.975	0.015	0.975
0.004	0.973	0.015	0.973
0.004	0.972	0.013	0.972
0.004	0.970	0.013	0.970
0.010	0.969	0.006	0.969
0.011	0.967	0.004	0.967
0.011	0.966	0.004	0.966
0.010	0.965	0.004	0.965
0.010	0.963	0.009	0.963
0.009	0.962	0.012	0.962
0.004	0.960	0.015	0.960
0.003	0.959	0.021	0.959
0.003	0.957	0.021	0.957
0.003	0.956	0.021	0.956
0.002	0.955	0.019	0.955
0.002	0.953	0.018	0.953
0.010	0.952	0.008	0.952
0.013	0.950	0.011	0.950
0.013	0.949	0.011	0.949
0.013	0.948	0.011	0.948
0.013	0.946	0.014	0.946
0.013	0.945	0.016	0.945
0.010	0.943	0.016	0.943
0.010	0.942	0.014	0.942
0.010	0.941	0.011	0.941
0.008	0.939	0.006	0.939
0.008	0.938	0.006	0.938
0.008	0.937	0.006	0.937
0.008	0.935	0.006	0.935
0.011	0.934	0.016	0.934
0.011	0.933	0.016	0.933
0.011	0.931	0.014	0.931

APPENDIX A2
(CONTINUED)

0.011	0.930	0.014	0.930
0.011	0.929	0.014	0.929
0.010	0.927	0.016	0.927
0.008	0.926	0.019	0.926
0.008	0.925	0.020	0.925
0.008	0.923	0.020	0.923
0.008	0.922	0.020	0.922
0.008	0.921	0.020	0.921
0.008	0.919	0.019	0.919
0.007	0.918	0.020	0.918
0.007	0.917	0.020	0.917
0.008	0.916	0.023	0.916
0.015	0.914	0.024	0.914
0.015	0.913	0.024	0.913
0.016	0.912	0.024	0.912
0.016	0.910	0.020	0.910
0.018	0.909	0.016	0.909
0.018	0.908	0.016	0.908
0.016	0.907	0.014	0.907
0.018	0.905	0.014	0.905
0.022	0.904	0.014	0.904
0.026	0.903	0.005	0.903
0.026	0.902	0.004	0.902
0.023	0.900	0.004	0.900
0.023	0.899	0.005	0.899
0.022	0.898	0.005	0.898
0.022	0.897	0.005	0.897
0.023	0.895	0.005	0.895
0.025	0.894	0.005	0.894
0.026	0.893	0.005	0.893
0.025	0.892	0.005	0.892
0.025	0.890	0.000	0.890
0.023	0.889	0.000	0.889
0.016	0.888	0.014	0.888
0.014	0.887	0.004	0.887
0.016	0.885	0.004	0.885
0.025	0.884	0.013	0.884
0.025	0.883	0.014	0.883
0.016	0.882	0.014	0.882
0.016	0.881	0.013	0.881
0.009	0.879	0.013	0.879
0.009	0.878	0.014	0.878
0.008	0.877	0.014	0.877
-0.004	0.876	0.013	0.876
-0.004	0.875	0.009	0.875
0.008	0.874	0.009	0.874
-0.002	0.872	0.008	0.872
-0.004	0.871	0.003	0.871

APPENDIX A2
(CONTINUED)

-0.004	0.870	0.003	0.870
-0.006	0.869	0.008	0.869
-0.008	0.868	0.003	0.868
-0.008	0.867	-0.002	0.867
-0.008	0.865	-0.017	0.865
-0.008	0.864	-0.023	0.864
-0.002	0.863	-0.026	0.863
0.006	0.862	-0.023	0.862
-0.002	0.861	-0.023	0.861
0.006	0.860	-0.004	0.860
0.006	0.859	-0.004	0.859
0.013	0.857	-0.004	0.857
0.014	0.856	-0.004	0.856
0.017	0.855	-0.004	0.855
0.020	0.854	0.003	0.854
0.029	0.853	0.008	0.853
0.039	0.852	0.008	0.852
0.020	0.851	0.008	0.851
0.017	0.850	0.017	0.850
0.017	0.848	0.028	0.848
0.014	0.847	0.028	0.847
0.014	0.846	0.017	0.846
-0.003	0.845	0.003	0.845
-0.018	0.844	0.017	0.844
-0.018	0.843	0.028	0.843
-0.018	0.842	0.028	0.842
-0.018	0.841	0.028	0.841
-0.018	0.840	0.028	0.840
-0.012	0.839	0.028	0.839
-0.004	0.837	0.028	0.837
-0.003	0.836	0.000	0.836
0.000	0.835	0.000	0.835

BIBLIOGRAPHY

[1] E. Yablonovitch, "Photonic Crystals", Phys. Rev. Lett. 58, p1059 (1987).

[2] J. D. Joannopoulos, Pierre R. Villeneuve & Shanhui Fan, "Putting a New Twist on Light", Nano News, April (1997).

[3] Science, "Making light of computers", 286, p 2227 December (1999).

[4] The British Broadcasting Corporation (BBC), January (2000). http://www.bbc.co.uk

[5] S. Lin, E. Chow, V. Hietala, "Sandia Photonic crystal bends micorwaves around a tight corner", Sandia Lab News, Vol. 50, No. 20, October (1998).

[6] M. Scalora, P. Sieck, "Light Constructions", Article EE Times, November (1999).

[7] J. G. Fleming, Shawn-Yu Lin, "Three-dimensional photonic crystal with a stop band from 1.35 to 1.95 μm" Optics Letters, Vol. 24, No. 1, January (1999).

[8] S. Y. Lin, J. G. Fleming, D. L. Hetherington, B. K. Smith, R. Biswas, K. M. Ho, M. M. Sigalas, W. Zubrzycki, "A three-dimensional photonic crystal operating at infrared wavelengths", Nature Vol. 394, No. 25 (1998).

[9] E. Ozbay, A. Abeyta, G. Tuttle, M. Tringides, R. Biswas, C. T. Chan, C. M. Soukoulis, K. M. Ho, "Measurement of a three- dimensional photonic band gap in a crystal structure made of dielectric rods, Nature Vol. 391, No. 23 (1998).

[10] E. Yablonovitch, "Photonic band-gap structures", J. Opt. Soc. Am. B, Vol. 10, No. 2 (1993).

[11] K. Ming Leung, Yang Qiu, "Two Dimensional Metallic Photonic Crystals", App. Phy. Soc. S15-Photonic Crystals, March (1998).

[12] Andrew L Reynolds, "Photonic Band Gap Materials Research", Electrical and Electronic Engg. Dept. University of Glasgow, UK.

[13] N. M. Albuquerque, "Photonic Crystals Trap IR Light", Photonic Technology News, September (1998).

[14] D. N. Chigrin, A.V. Lavrinenko, "Multilayer periodic structures as an all-angle photonic insulator", in Conference Program of the 1998 OSA Annual Meeting and Exhibit, Baltimore, Maryland, USA, p. 118, (1998).

[15] Sunny Bains, "Infrared photonic crystals fabricated using deep x-ray lithography", SPIE OE Reports 169, January (1998).

[16] D. N. Chigrin, A. V. Lavrinenko, "Existence of total omnidirectional reflection from one-dimensional periodic dielectric structures", Phys. Rev. Lett. June, (1998).

[17] D. N. Chigrin, A. V. Lavrinenko, D. A. Yarotsky, and S. V. Gaponenko, "Observation of total omnidirectional reflection from a one-dimensional dielectric lattice", Appl. Phys. A, Vol. 68, pp. 25-28, (1998).

[18] D. A. Yarotsky, and S. V. Gaponenko, D. N. Chigrin, A. V. Lavrinenko, "Observation of omnidirectional reflection from a one-dimensional dielectric lattice", in Conference Program of the Workshop on Electromagnetic Crystal Structures, Design, Synthesis, and Applications, Laguna Beach, California, USA, (1999).

[19] Sunny Bains, "Holographic lithography yields photonic crystals", Electronic Times, September, (2000).

[20] Kai-Ming Ho, Rana Biswas, Mihail Sigalas, Ihab El-Kady, Dave Turner, Costas Soukoulis, Gary Tuttle, Kristen Constant, "Photonic Bandgap Structures", Ames Laboratory.

[21] P. Yeh, "Optical Waves in Layered Media", Chap 5, Wiley, New York (1998).

[22] J.P. Hebb, K. F. Jensen, "Photonic crystals", J. Electrochem. Soc., 143, 1142 (1996).

[23] R. Siegel, J. R. Howell, "Thermal Radiation Heat Transfer", Hemisphere Publishing Corporation, Washington, D.C. (1992).

[24] D. P. DeWitt and G. D. Nutter, "Theory and Practice of Radiation Thermometry", Wiley, New York, (1998).

[25] G. E. Jellison, F. A. Modine, "Photonic crystals", J. Appl. Phys., 76, 3758 (1994).

[26] P. J. Timmans, "Photonic crystals", J. Appl. Phys., 74, 6353 (1993).

[27] G. G. Macfarlane, T. P. McLean, J. E. Quarrington and V. Roberts, "Photonic crystals", Phys. Rev., 111, 1245, (1958).

[28] Handbook of Optical constants of Solids, ed. E. Palik, Academic Press, New York, (1985).

[29] A. N. Magunov, "Photonic crystals", Opt. Spectrosc., 73, 205, (1992).

[30] G. Burns, Solid State Physics, Academic Press Inc., New York, Chap. 13, (1990).

[31] C. D. Thurmond, "Photonic crystals", J. Electrochem. Soc., 122, 1133, (1975).

[32] F. J. Morin, J. P. Maita, "Photonic crystals", Phys. Rev., 96, 28, (1954).

[33] J. C. Strum, Reaves, "Photonic crystals", IEEE Trans. Electron Devices, 39, 81 (1992).

[34] J. D. Joannopoulos, R. D. Meade, J. N. Winn, Photonic Crystals, "Molding the Flow of Light", Princeton University Press, (1995).

[35] E. Yablonovitch, " Photonic band-gap structures", J. Opt. Soc. Am. B, Vol. 10, No. 2, February, (1993).

[36] J. B. Bates, "Fourier transform infrared spectroscopy", Science, Vol. 191, No. 4222, 31, January, (1976).

[37] J. R. Markham, K. Kinsella, R. M. Carangelo, C. B. Brouillitte and P. R. Solomon, "A bench top FT-IR based instrument for simultaneously measuring surface spectral emittance and temperature", Rev. Sci. Instrum., Vol. 64, No. 9, 2515, September, (1993).

[38] Thomas Piok, Charles Brands, Patrick J. Neyman, Artur Erlacher, Charuta Soman, Mary A. Murray, Raoul Schroeder, James R. Heflin, Willi Graupner, Daniela Marciu, Adam Drake, M.B. Miller, Hong Wang, Harry W. Gibson, and Harry C. Dorn, Guenter Leising, Mathew T. Guzy and Richie M. Davis, "Efficient charge generation in conjugate molecules", PMSE 258, August, (2000).